UCLouvain

École polytechnique de Louvain

Increasing the share of renewable sources through hydrogen:

Optimisation and uncertainty quantification of a Power-to-Hydrogen system under stochastic conditions

Authors : **Florent MELOTTE**
Supervisors : **Francesco CONTINO**, **Kevin VERLEYSEN**
Readers : **Emmanuel DE JAEGER**
Academic year 2021–2022
Master [120] in Mechanical Engineering

Abstract

As part of the fight against global warming, a general transition from fossil fuels to renewable energies is taking place. However, this is hindered by the intermittent nature of renewable energies, which limits their use. To overcome this problem, many storage methods have emerged. Amongst these solutions is hydrogen, which is particularly well known for its potential carbon neutrality and high energy density. The surplus energy generated by renewable sources can be recovered by converting it into hydrogen through the electrolysis of water via various technologies. A literature review on these different technologies was carried out to identify the most suitable one to be coupled with a volatile power source. This shows that the Proton Exchange Membrane electrolyser (PEM El) is the most suitable for dynamic operating conditions. However, the electrolyser achieves low efficiency at high load factors and suffers significant degradation under dynamic conditions. To overcome this problem, the electrolyser was coupled to batteries in order to operate only within a certain range of load factors.The batteries charge with the excess energy and discharge when the power supplied by the renewable source is low. When they run out of energy, the electricity grid supplies power to the electrolyser so that it does not shut down. In this report, the renewable energy source is simulated by a stochastic process, the Ornstein- Uhlenbeck (O-U) Geometric Brownian Motion (GBM) model. It allows to study the impact of the wind speed uncertainty on the system performance. For this purpose, the system was subjected to deterministic optimisation using a Nondominated Sorting Genetic Algorithm II (NSGA-II) with three objectives: minimising grid usage and losses when the batteries are full (grouped into a single objective), maximising the lifetime of the electrolysers and finally maximising the lifetime of the batteries. Then, an uncertainty quantification was performed on several designs with a Polynomial Chaos Expansion (PCE). The results showed that there is a real trade-off between flexibility and degradation of the electrolysers. However, a design that minimised the amount of grid and loss, with acceptable degradation, was found to be more robust than a design that minimised degradation.

Contents

List of Figures

List of Tables

Chapter 1

Introduction

As global energy consumption continues to grow, the world is striving to reduce Green House Gases (GHG) emissions as much as possible [1]. The undeniable cause of this GHG is the heavy dependence of our system on fossil fuels. In 2021, 82% of the world's primary energy was produced from fossil fuels and more than 61% of electricity production [2]. In the hope of reducing this dependence, all eyes are on renewable energies. To be respected, the Paris agreement calls for renewable energy to be responsible for almost two-thirds of global energy production by 2050. Indeed, clean and infinite, it seems to be the ideal solution to the problem the world is facing. This is without consider its intermittency which makes its exploitation complicated because of its lack of concordance with the energy demand. The sun sleeps at night and rests in winter, while the wind is more unpredictable than ever.

The question today is not so much how to convert this energy but rather how to handle it and adapt it to our system? The most common solution is to store the excess energy so that it can be shifted in time. One possibility is to convert electrical energy into chemical energy. This thesis focuses on the storage of electrical energy into chemical energy as hydrogen. Since the transport and industrial sectors will always need combustible fuel, this need can be met by hydrogen itself produced by renewable energies. In this way, hydrogen can spread the influence of renewable sources to areas where electrification is not sufficient to meet energy needs. To this end, this work focuses on the production of hydrogen powered by a wind farm through the Power-to-Hydrogen so called process.

Chapter 2

Hydrogen

2.1 Power to Hydrogen

In the current fight against global warming, there is a need to increase the share of renewable energy in our energy system [4]. Indeed, despite the fact that all this energy is offered to us free of charge by nature, there remains a problem, its intermittency [7]. This prevents us from exploiting its full potential by a lack of concordance with the energy demand. However, there is a solution to every problem, and this thesis focuses on one of them, the Power to hydrogen [5]. To overcome this lack of synchronization, the main idea is to store this energy to facilitate the flexibility of its use. The storage methods are multiple but the one we are particularly interested in is hydrogen. Our universe is made up of a multitude of chemical elements, among which hydrogen is the simplest and lightest atom. It represents 75% of matter, which makes it one of the most abundant chemical substances. Its mass energy density, which is three times greater than that of hydrocarbons such as petrol or diesel, makes it a credible candidate for all kinds of uses [6]. But beyond the interesting energy characteristics of the dihydrogen molecule, it is above all its potential to de-carbonise many sectors that is attractive [6]. Indeed, there are many uses for this atom and it seems important for the scientific world to explore them in greater depth to bring out the best of hydrogen. The use of hydrogen to store the surplus energy produced by intermittent renewable energies has attracted a lot of interest in recent years [8]. For many, it is one of the major keys to enabling the de-carbonisation of our energy system. The general principle of Power to hydrogen consists in the transformation of electrical energy into chemical energy in the form of hydrogen [9]. The main advantage of chemical energy is its non-instantaneous nature, unlike electricity [10, 11]. Thus, the use of the energy produced by the renewable source has the possibility to be shifted in time. Indeed, the hydrogen obtained can either be converted again into electricity when the demand is important or simply be used as fuel for many applications. In the framework of this thesis, the renewable energy source is completely devoted to the production of hydrogen, i.e. all the generated power is used for this purpose. In order to achieve this energy conversion, the electrolysis method takes place.

2.1.1 Electrolysis

Electrolysis is an endothermic electrochemical process that converts electrical energy into chemical energy. This technique requires a direct current (DC) supply to generate a non-spontaneous chemical reaction. In short, as its ethymology indicates, the word ("lysis" meaning separation), electrolysis separates by electricity [12]. In the specific case of hydrogen, it is the electrolysis of water that interests us. This allows the dissociation of the water

molecule into hydrogen and oxygen. The general principle consists of two electrodes placed in the water, the anode and the cathode, through which electrons pass [13]. Hydrogen appears at the cathode while oxygen appears at the anode. The overall reaction of water electrolysis is as follows:

$$H_20(l) \rightarrow H_2(g) + O_2(l) \tag{2.1}$$

Two water molecules produce two hydrogen molecules and one oxygen molecule. Although it is the hydrogen that interests us, oxygen can also be used in certain sectors. There are currently three main families of electrolysers with very different characteristics. It is necessary to identify the most appropriate electrolyser for the situation under consideration by reviewing the main current technologies.

2.1.2 Alkaline water electrolysis

Alkaline water electrolysis (AWE) technology is certainly the most mature and widespread of the technologies presented. With many years of experience under its belt, it is responsible for the majority of the hydrogen produced today [15]. Indeed, the main advantage of AWE is the possibility of reaching outputs of several megawatts for each electrolyser stack. From a technical point of view, its electrodes are immersed, as the name suggests, in an alkaline elctrolyte solution mixed with water [16, 17]. This is mainly a potassium hydroxide (KOH) solution with a concentration of between 20 and 40%. The water separates at the cathode into hydroxide ions and hydrogen, after which the hydroxide ions pass to the anode before reacting to produce water and oxygen (Figure 2.1. In summary, the different reactions in an AWE are as follows :

$$Cathode : 2H_2O(l) + 2e^- \Longrightarrow H_2(g) + 2OH^-(aq) \tag{2.2}$$

$$Anode : 2OH^-(aq) \longrightarrow \frac{1}{2}O_2(g) + H_2O(l) + 2e^- \tag{2.3}$$

A diaphragm also separates the two electrodes to prevent mixing of the gases [18]. This, however, involves a large ohmic resistance reducing the operating range of the electrolyser to less than $0.5[A/cm^2]$. In addition, the AWE has a much longer response time than other available technologies, making its flexibility to a volatile power source very low [19, 20]. Despite this, it remains a cheap technology compared to its neighbours and is well suited to hydrogen production where the power source is more or less constant.

2.1.3 Proton-exchange membrane electrolysis

This technology is more recent than AWE but is already well developed [21]. This one, while having the same objective of producing hydrogen, works differently. The main part is its proton exchange membrane (PEM) placed between the two electrodes. Water in contact with the anode separates into oxygen, H^+ protons and electrons when a sufficient potential is applied across the electrodes [22]. The protons travel to the cathode through the proton exchange membrane and recombine with the electrons to form hydrogen (Figure 2.2). The oxidation and reduction reactions taking place in the cell are as follows:

$$Cathode : 2H_20(l) \Longrightarrow \frac{1}{2}O_2(g) + 2H^+ + 2e^- \tag{2.4}$$

$$Anode : 2OH^- \longrightarrow \frac{1}{2}O_2 + H_2O + 2e^- \tag{2.5}$$

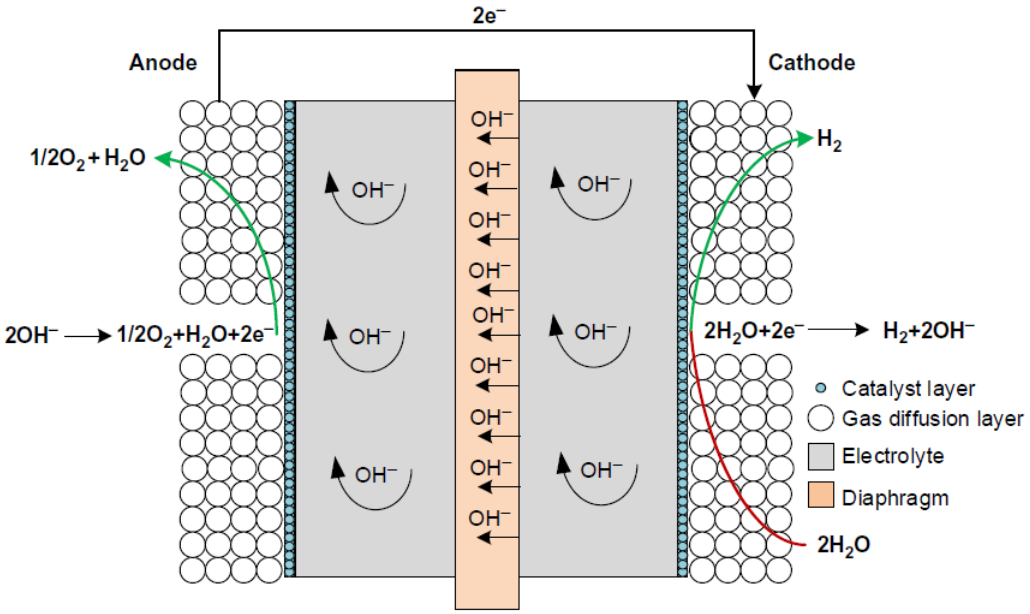

Figure 2.1: Alkaline water electrolyser from [14]

The role of the alkaline electrolyte liquid is therefore replaced here by the solid membrane . This also prevents the mixing of gases on both sides. The geometry of the membrane has a significant impact on the performance of the cell [23]. The main negative point of this technology is its necessary investment cost, which is twice that of AWE. In addition, it is subject to greater degradation, which is not yet fully understood, and which can considerably reduce its lifetime [24]. Beyond these negative points, PEM electrolysis has been rapidly developed for the numerous advantages it brings. First of all, it is possible to achieve high current densities, thus extending the operating range of the installation. This makes it possible to respond to the higher power levels typically found in renewable sources [9]. Furthermore, the transient behaviour is very fast compared to AWE. Indeed, the response to a power variation is of the order of a few tens of seconds maximum [25]. These characteristics seem at first sight suitable for coupling intermittent energy sources.

2.1.4 Solid oxide electrolysis

The electrolyte used is ceramic, more precisely solid oxides. The main objective is to reduce the energy required for the separation of water by means of particularly high operating temperatures ($500 - 900[°C]$) [27]. In this case, the water is obviously in the form of steam. This is fed to the cathode to be split into hydrogen and oxygen anions in a reduction reaction. The hydrogen leaves the cell through the cathode while the oxygen anions pass through the electrolyte to recombine with two electrons at the anode to form oxygen (Figure 2.3). A high density of electrolysis is required to prevent hydrogen and oxygen from recombining at the anode [28]. The different reactions taking place in the cell are the following:

$$Cathode : 2H_2O(g) + 2e^- \Longrightarrow H_2(g) + O^{2-}(g) \tag{2.6}$$

$$Anode : O^{2-} \longrightarrow \frac{1}{2}O_2(g) + 2e^- \tag{2.7}$$

The aim here is to consume less electricity through a high operating temperature that reduces the required electrical potential. In order to operate under such conditions, it is possible to

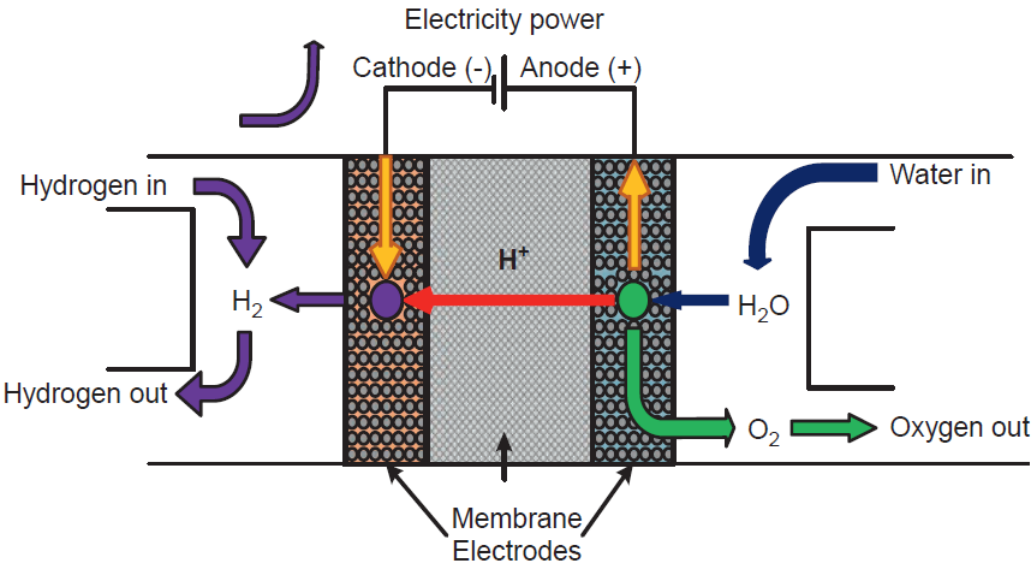

Figure 2.2: Proton Exchange Membrane from [14]

couple this system to sources of waste heat in industry or energy production (nuclear power plant, engines,..) [29]. Apart from this gain in efficiency, SOE technology remains in the development stage due to its rapid degradation under extreme operating conditions. It is nevertheless interesting to keep an eye on its evolution over the next few years, as its potential is no longer to be demonstrated.

2.1.5 What technology for power to hydrogen?

Now that the main technologies available have been presented, it is necessary to identify the most suitable one for coupling to a typical intermittent power source such as a wind turbine. SOE has much higher efficiencies but, in addition to its premature degradation, is still in the development stage. The maximum power output of a stack of SOE electrolysers is far too low to be of interest on a large scale, unlike alkaline technology, which accepts power outputs of $6MW$. However, despite this large-scale use and a great deal of knowledge about it, it is limited by its low limiting current density and its too long reaction time in case of power variation. For these reasons it seems obvious that the PEM electrolyser is the most suitable for such use. Despite its rather high investment cost, it is the only mature technology capable of responding quickly to a power variation at its input. The rest of the work will therefore focus solely on proton exchange membrane electrolysis technology. This will be modelled in order to reproduce its behaviour as closely as possible to reality. Table 2.1 summarises the main characteristics of the technologies mentioned above.

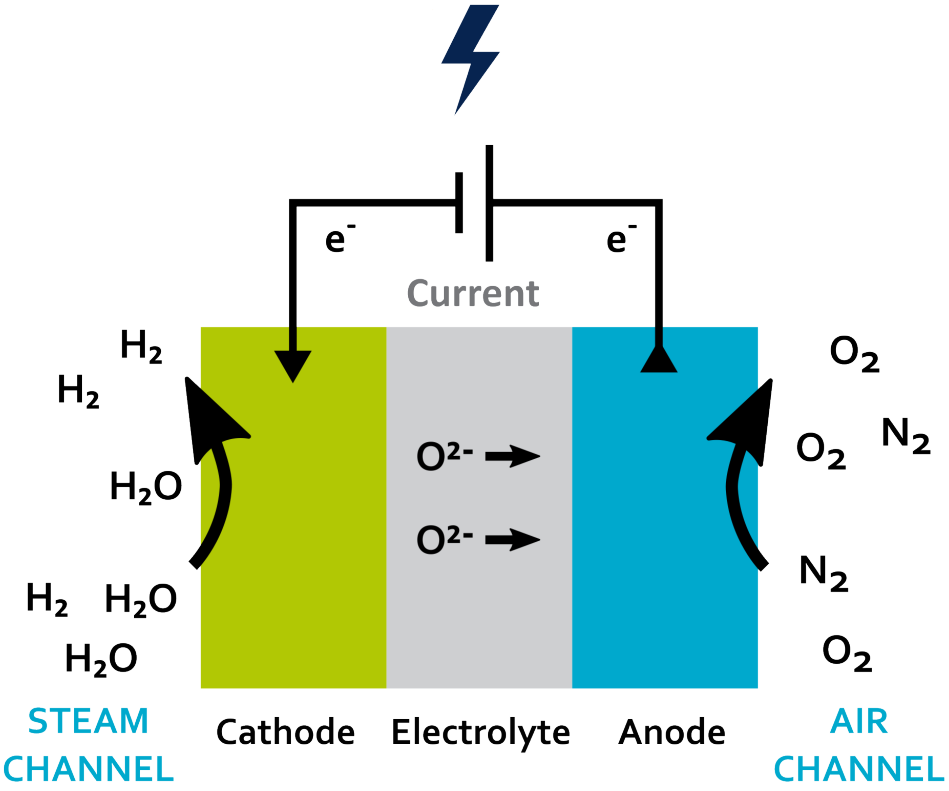

Figure 2.3: Solid oxide electrolyser cell from [26]

	Alkaline	PEM	SOE
Temperature $[°C]$	60-90	30-80	500-900
Current density $[Acm^{-}2]$	0.25-0.45	0.1-2.0	0.3-1.0
Warm start up time	1-5min	<10s	15min
Stack Power $[MW]$	6	2	<0.01
Investment cost $[€kW^{-1}]$	800-1500	1400-2100	>2000

Table 2.1: Comparison of characteristics between the different technologies presented based on Butler et al. work [30]

Chapter 3

System model

This chapter presents the general system used in the simulations. As a reminder, the objective of this thesis is to study the flexibility of a hydrogen power system with an input power following a stochastic process similar to an intermittent renewable source. In this study, the simulated renewable source is a wind farm. The stochastic process provides wind speeds that must be converted into power. The objective is therefore to know how the system reacts to the volatility of its input power. In addition to the electrolysers, it was decided to integrate batteries into the system in order to study the influence they may have on the objectives described later. The last element to be considered is the electrical grid, which could be used as a backup power during the simulations.

3.1 System scenarios

This section is intended to explain clearly to the reader how the system reacts to the power generated and to certain parameters. The first essential thing to know is that the electrolyser is set up to stay within a certain operating range. This means that a minimum power P_{min} and a maximum power P_{max} are set at the beginning of the simulation, beyond which the electrolyser will never operate. When the power generated is beyond this range, the battery and the electrical network are there to absorb/supply the excess/shortage of power. It is now possible to analyse the different scenarios encountered by the model during simulation.

Scenario 1: Power generation within the operation range

In the first and simplest case, the power generated by the wind farm P_{WF} is within the range initially set for the electrolyser.

$$P_{min} < P_{WF} < P_{max} \tag{3.1}$$

The system therefore simply sends the generated power to the electrolyser to produce hydrogen.

$$P_{WF} = P_{Electrolyser} \tag{3.2}$$

In this scenario, the electrical network and the batteries are not used at all (3.1).

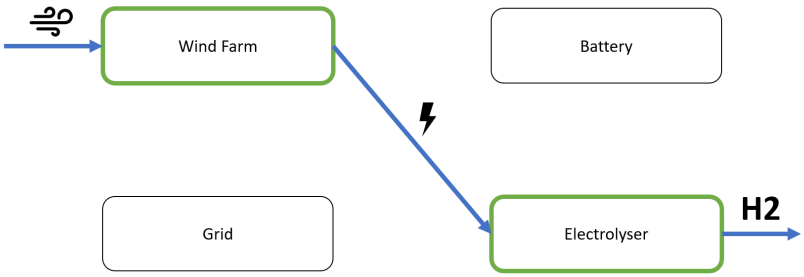

Figure 3.1: Scenario 1: The power generated by the wind farm is in the operation range of the electrolyser. The power is therefore directly used for hydrogen production.

Scenario 2: Power generation above the operation range

When the power generated by the wind farm is greater than the operating range, it splits in two (3.2).

$$P_{WF} > P_{max} \tag{3.3}$$

The maximum power allowed in the electrolyser is supplied to it while the surplus is redirected to the batteries.

$$P_{WF} = P_{max} + P_{Battery} \tag{3.4}$$

Where,

$$P_{Electrolyser} = P_{max} \tag{3.5}$$

In this scenario the batteries are charged with the surplus power generated. If the batteries no longer have the required capacity to store energy, the energy produced by the wind farm is adjusted.

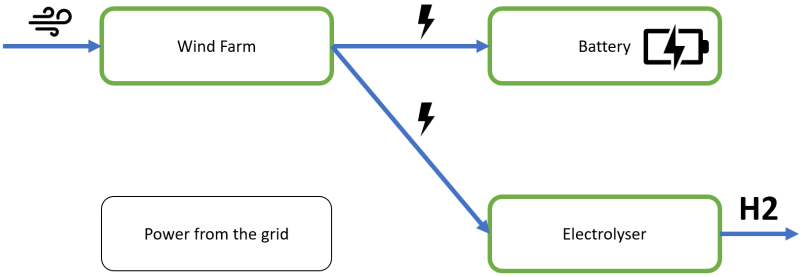

Figure 3.2: Scenario 2: The power generated is above the operation range. Batteries are storing the excess of power.

Scenario 3: Power generation below the operation range with charged battery

In this third scenario, the power generated by the wind farm is lower than the minimum power allowed bys of the electrolyser.

$$P_{WF} > P_{min} \tag{3.6}$$

When there is enough energy is the battery, it is used to compensate for the lack of power generated (figure 3.3). The input power to the electrolyser here comes from two different

sources.

$$P_{Electrolyser} = P_{min} = P_{WF} + P_{Battery} \tag{3.7}$$

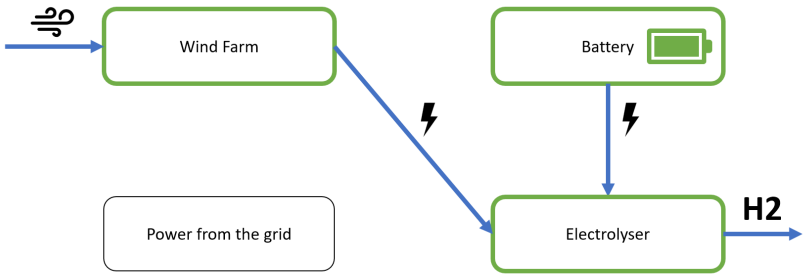

Figure 3.3: Scenario 3: The power generated is below the operation range. Batteries compensate this lack of power in the electrolysers wich produce hydrogen

Scenario 4: Power generation below the operation range with empty battery

This last scenario is equivalent to the third (3.6) with the only difference that battery does not have enough energy stored. The system is then forced to use the electrical grid in order to maintain the electrolyser at minimum power (figure 3.4). Although using the electrical grid may seem unnecessary, this strategy ensures that the electrolyser is never switched off to avoid start-up procedures. The power for the electrolyser is therefore provided by the wind farm and the electrical grid.

$$P_{Electrolyser} = P_{WF} + P_{Grid} = P_{min} \tag{3.8}$$

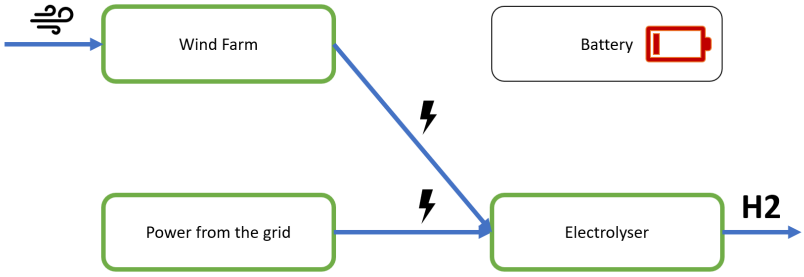

Figure 3.4: Scenario 4: Power generation below the operation range with empty battery

3.2 Wind farm power generation

In this thesis, the renewable energy source supplied to the electrolyser is a wind farm. Wind was chosen over solar for its much more volatile and less predictable nature in order to analyse the impact of this intermittency on the flexibility of the electrolyser. Rather than retrieving power data already generated by an existing wind farm, a stochastic process was used to obtain wind speeds in the most realistic way possible. The stochastic process has the advantage that many different wind speed profiles can be generated in order to study the impact of variability. While using a single power profile at the input of the electrolyser would not allow to observe the influence of time-variant uncertainties. Once the wind speed

data is collected, it needs to be converted into power using a typical wind turbine power profile. The NREL5MW wind turbine from the National Renewable Energy Laboratory was used to perform this conversion [32]. The stochastic process is presented in a first step. The explanation of the wind turbine used to convert the wind into electrical power is presented in a second step.

3.2.1 Stochastic process

The stochastic process for generating the wind speeds was provided by my supervisor Kevin Verleysen hich mainly based on the work of Angeliki Loukatou et al [31]. First of all it is interesting to know why we model wind speeds and not directly the power generated by the wind farm. In fact it is quite simple, unlike the wind, the power generated by a wind turbine does not follow a precise distribution because it is bounded by its minimum and maximum operating power. That is why it is best to model the wind first and convert the data. The wind speed $V(t)$ is modelled by an Ornstein-Uhlenbeck (O-U) Geometric Brownian Motion (GBM) model of a log-wind speed data which is decomposed into a daily deterministic cycle $f(t)$ and short-term variations $Y(t)$.

$$lnV(t) = f(t) + Y(t) \tag{3.9}$$

The deterministic part $f(t)$ is fitted with Fourier series while the stochastic component $Y(t)$ is modelled by an O-U process. It should be noted that the future variance of the wind speeds remains bounded and does not evolve with time. To the equation 3.10 it remains to isolate $X(t)$ in order to obtain the wind speed at each time t.

$$V(t) = \exp(f(t) + Y(t)) \tag{3.10}$$

These explanations are the basis of the stochastic process which remains a black box, in the framework of this thesis, for which it is possible to vary some input parameters. Among these we find the time period T over which we wish to obtain the velocity data, the time step t_s which corresponds to the time interval between each data and the uncertainty coefficients ϵ. These each follow a Gaussian distribution centred at zero with a unit variance. Subsequently, the impact of these coefficients on the system objectives will be analysed in order to draw conclusions on the influence of the unpredictability of the wind. The number of ϵ coefficients provided to the O-U process, responsible for the stochasticity, greatly influences the generated velocity profile. Too few coefficients result in an unrealistic curve due to too few uncertainties.

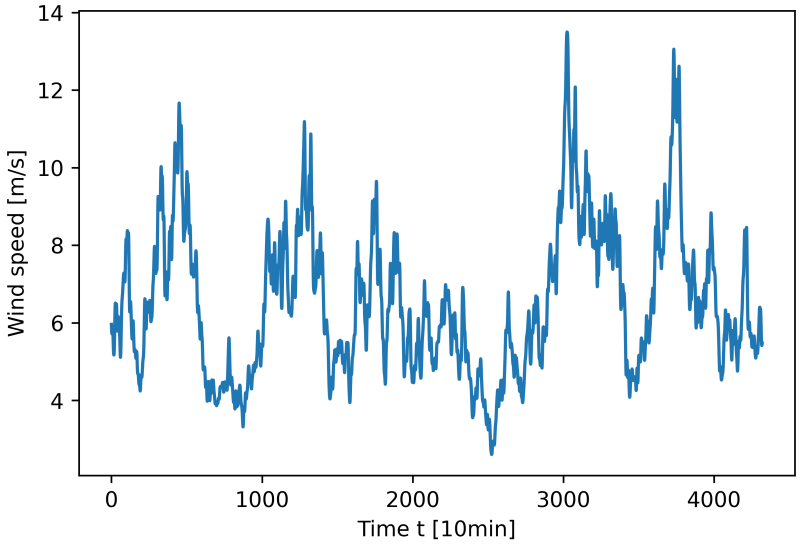

Figure 3.5: Wind profile generated by the Ornstein-Uhlenbeck (O-U) Geometric Brownian Motion (GBM)

As an example, I have generated wind speeds over a thirty day period with a time step of ten minutes (Figure 3.5). In order to check the realism of the data, it is possible to draw the monotonic function (Figure 3.6) of these. The monotonic function obtained corresponds to the observations made on experimental data.

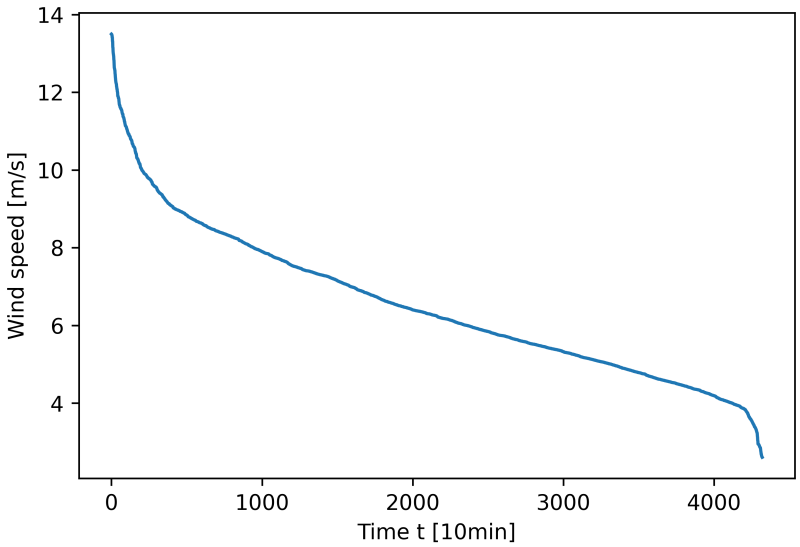

Figure 3.6: Monotonic function of the windspeed

3.2.2 Power conversion

The conversion of the wind speed profile generated by the stochastic process into a power profile is based on the NREL5MW wind turbine of the National Renewable Energy Laboratory. All the necessary data for the conversion is available in this paper [32]. The power profile of a wind turbine can be defined in 6 distinct regions according to the wind speeds encountered at the turbine blades.

Region 1

In this region, the wind speed is lower than the minimum speed allowed by the wind turbine.

$$V_{wind} <= V_{min} \tag{3.11}$$

The turbine therefore stops operating below this value and the power generated is zero.

$$P_{WF,1} = 0 \tag{3.12}$$

It is a control region before cut-in where the wind is use to accelerate the rotor for start-up.

Region 1/2

It's a start up region making a linear transition between region 1 and region 2 where :

$$V_{min} < V_{wind} < V_1 \tag{3.13}$$

The power extracted in this region is :

$$P_{WF,1/2} = \frac{K\ (\frac{N\ TSR}{R})^3(\frac{30}{\pi})^2 V_1^3 (V_{wind} - V_{min})}{(V_1 - V_{min})} \tag{3.14}$$

Where TSR is the optimal tip speed ratio of the wind turbine, K is the optimal constant of propotionality between torque and rpm, N is the gearbox ratio and R is the blade radius of the wind turbine.

Region 2

Region 2 optimized the power capture by maintaining a constant tip speed ratio when the wind speed is:

$$V_1 < V_{wind} < V_2 \tag{3.15}$$

The power extracted is function of the wind speed.

$$P_{WF,2} = K\ \left(\frac{N\ TSR}{R}\right)^3 \left(\frac{30}{\pi}\right)^2 V_{wind}^3 \tag{3.16}$$

Region 2/3

This region is a linear between region 2 and region 3. It is needed to limit tip speed and rated power.

$$P_{WF,2/3} = \frac{P_{rated} - K\ (\frac{N\ TSR}{R})^3(\frac{30}{\pi})^2 V_2^3}{(V_{max} - V_2)}(V_{wind} - V_2) + K\ \left(\frac{N\ TSR}{R}\right)^3 \left(\frac{30}{\pi}\right)^2 V_2^3 \tag{3.17}$$

Where P_{rated} is the nominal power of the wind turbine.

Region 3

The third region keeps the extracted power constant while the wind speed is still increasing.

$$P_{WF,3} = P_{rated} \tag{3.18}$$

Region 4

The last region shuts down the turbine when the wind speed exceeds a limit beyond which it is unsafe for the turbine to operate with the risk of severe damage.

$$V_{wind} >= V_{max} \tag{3.19}$$

The power here is simply zero as in region 1.

$$P_{WF,4} = 0\ [W] \tag{3.20}$$

Power profile

Now that the different operating regions of the wind turbine have been defined. It is possible to convert the generated speed data (Figure 3.5) by the stochastic process into a power profile (Figure 3.7). Thus, at each simulation, a new power profile can be simulated in order to study the unpredictability of the wind on the system performances.

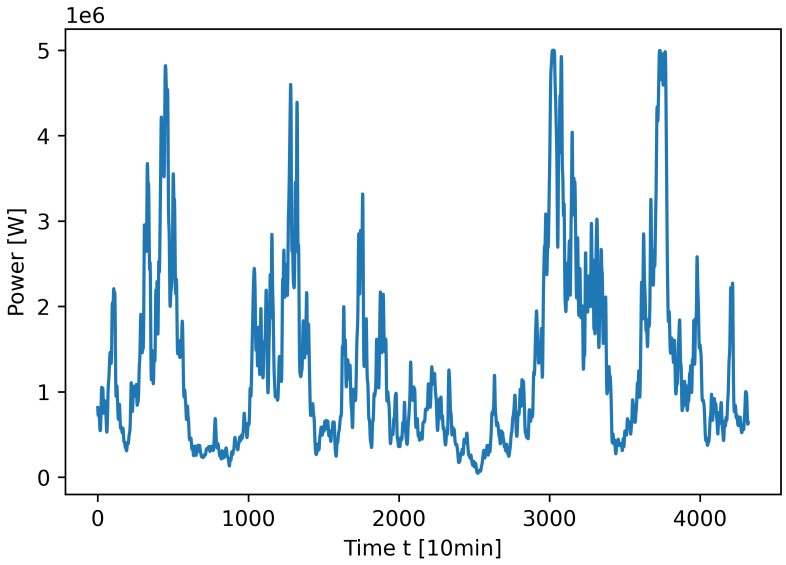

Figure 3.7: Power profile of the wind farm generated by NREL5MW wind turbine using the stochastic process to generate the wind speed

3.3 Electrolyser model

In this chapter, the overall structure of the electrolyser model is presented. Its objective is to simulate realistically the behaviour of an electrolyser subjected to large power variations at its input. It is therefore important to consider any phenomenon induced by such volatility. The presentation of the electrolyser is divided in 3 sections enabling to clearly identify the specific areas influencing the performance of the modelled electrolyser. The electrical section of the electrolyser seems to be the most essential as it is the central point of the electrolyser operation. Then, it is necessary to study the evolution of the temperature of the system, the thermal area, which has a direct impact on the performance of the system. Finally, there remains the fluidic domain identifying the molar flows present in the cell at each moment.

3.3.1 Electrical domain

The electrolyser, converts the energy supplied, in the form of current, into hydrogen. To achieve this conversion, sufficient energy is required to allow the separation of the hydrogen atom from the water molecule. The potential required between the anode and the cathode, under reversible conditions, is called the reversible potential noted E^0_{rev}. To quantify this energy we must use the Gibbs free energy (ΔG^0_r) corresponding to the global reaction across the electrodes. According to the PEM electrolyser, we find a value of 236 kJ/mol, the positive value of which effectively indicates that an energy input is necessary for the water separation reaction. Using the Faraday constant (F) and the number of electrons exchanged during the reaction (n), the reversible potential is defined as follows:

$$E^0_{rev} = \frac{\Delta G^0_r}{nF} = 1.229[V] \tag{3.21}$$

In order for the reaction to take place, a heat input is also required. Assuming that no heat source external to the electrolyser is used, it must be delivered using the available electrical energy. The reversible enthalpy (ΔH^0_R) under standard condition being 285 [kj/mol], the required electrical potential, called thermoneutral voltage, is defined as :

$$E^0_{tn} = \frac{\Delta H^0_R}{nF} = 1.481[V] \tag{3.22}$$

In summary, under reversible conditions, when a current flows through the cell, a higher potential is required than the thermoneutral voltage to ensure the separation of water into hydrogen. The total potential of the cell is in fact often much higher because of irreversible potential losses at different levels of the electrolyser. To model the behaviour of the cell in a realistic way, it is fundamental to know the evolution of these different potentials at each time step of the simulation. There are four main voltage drops characterising the overall cell voltage :

$$E_{cell} = E_{rev} + E_{act} + E_{diff} + E_{Ohm} \tag{3.23}$$

The reversible potential allowing water separation and three irreversible overpotentials resulting in a loss of efficiency of the electrolyser. The following sections are intended to clarify these different potentials.

Reversible Voltage

The reversible potential of the electrolyser corresponds to the energy required to allow the water to split into oxygen and hydrogen. As previously presented (3.21), under standard conditions this voltage is quantifiable using the Gibbs free energy. However, the conditions within the cell of the electrolyser are far from being regular, so it is necessary to adapt this value by considering temperature and partial pressures. The reversible potential is finally defined using the Nernst equation [35].

$$E_{rev} = E^0_{rev} + \frac{RT}{2F}\left(\frac{P_{H_2}P^{1/2}_{O_2}}{a_{H_2O}}\right) \tag{3.24}$$

Where T is the temperature within the cell, P_i the partial pressure of the reactants and products involved in the reaction and R = 8.314/K/mol the universal gas constant. The reversible potential under standard conditions is as shown in 3.21. However, following experiments carried out on the basis of PEM electrolysers, some authors have come to the conclusion that there is a certain dependence on the operating temperature as well. This

is why it was preferred to use an empirical expression (3.25) widely shared in the scientific literature for this reversible potential under standard conditions [37].

$$E^0_{rev} = 1.5241 - 1.2261\ 10^{-3}T + 1.1858\ 10^{-5}Tln(T) + 5.6692\ 10^{-7}T^2 \tag{3.25}$$

Henceforth, at each time step for a known operating temperature and partial pressures, it is possible to calculate the reversible potential necessary for the electrolysis reaction. In the case of this study, the partial pressure of the reactants and products is a fixed parameter at the beginning of the simulation, whereas the temperature evolves over time. It is therefore already interesting to observe the link between this reversible potential and the temperature to understand its behaviour during the simulations.

The increase in operating temperature leads to a decrease in the potential required for the same current through the membrane (Figure 3.8). This results in a decrease in the total power required for equivalent hydrogen production and therefore an increase in performance. The effect of irreversible potentials still needs to be added to confirm this positive influence of temperature.

Activation overpotential

Activation losses occur, as referred, because of the necessity to sacrifice some potential to activate the electrochemical reactions taking place at anode and cathode sides. There is a shift in the thermodynamic equilibrium which reduces the reaction rate. It can be determined, as at equation 3.26, by Butler-Volmer and Tafel's laws [36].

$$E_{act} = \frac{RT}{z\alpha F} ln\left(\frac{i}{i_0}\right) \tag{3.26}$$

Where i_0 is the exchange current density at the electrodes, α the charge transfer coefficient and i is the current density going through the cell. The exchange current density can be redefined taking into account the operating temperature :

$$i_0 = i_{0,ref} exp\left(-\frac{E_a}{R}(\frac{1}{T} - \frac{1}{T_{ref}})\right) \tag{3.27}$$

E_a is the activation energy of the electrode and $i_{0,ref}$ the exchange current density at reference temperature. The activation losses at the anode and electrode are defined by the same expression (3.26) but with different parameter values identifiable in the literature. Again, it can be seen that in addition to being a function of the current density, these activation losses are related to the operating temperature. As for the reversible potential, a decrease in activation losses occurs when the temperature increases for the same current density (Figure 3.9). This implies an increase in the performance of the cell cause the overpotential is lower at higher temperature. It is also observable that the losses at the anode are almost three times higher than those at the cathode (Figure 3.9).

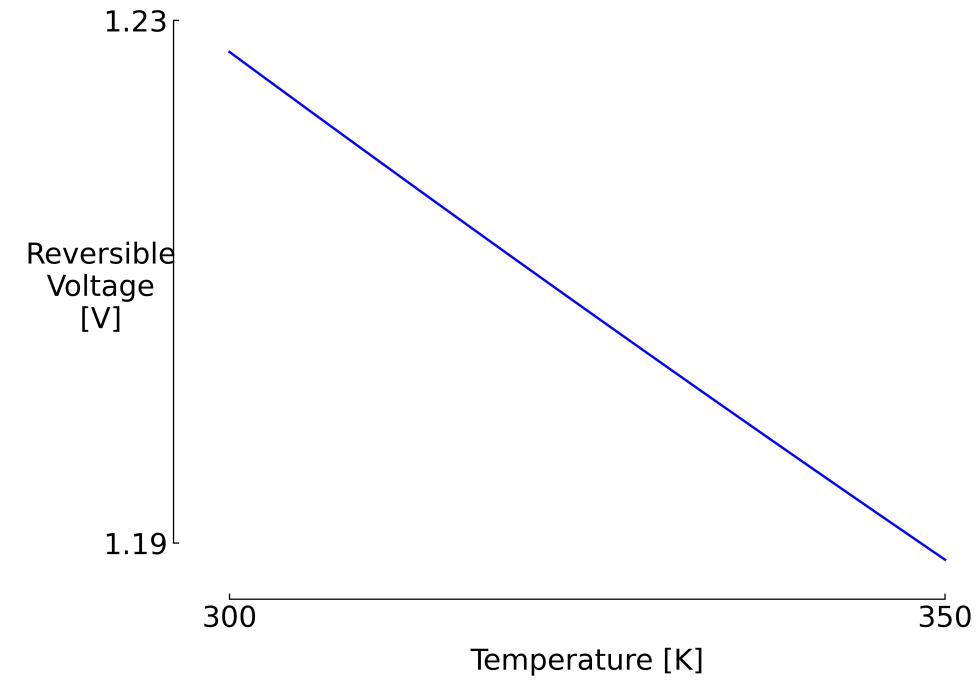

Figure 3.8: Evolution of the reversible potential [V] according to the operating temperature [K] for a constant current density

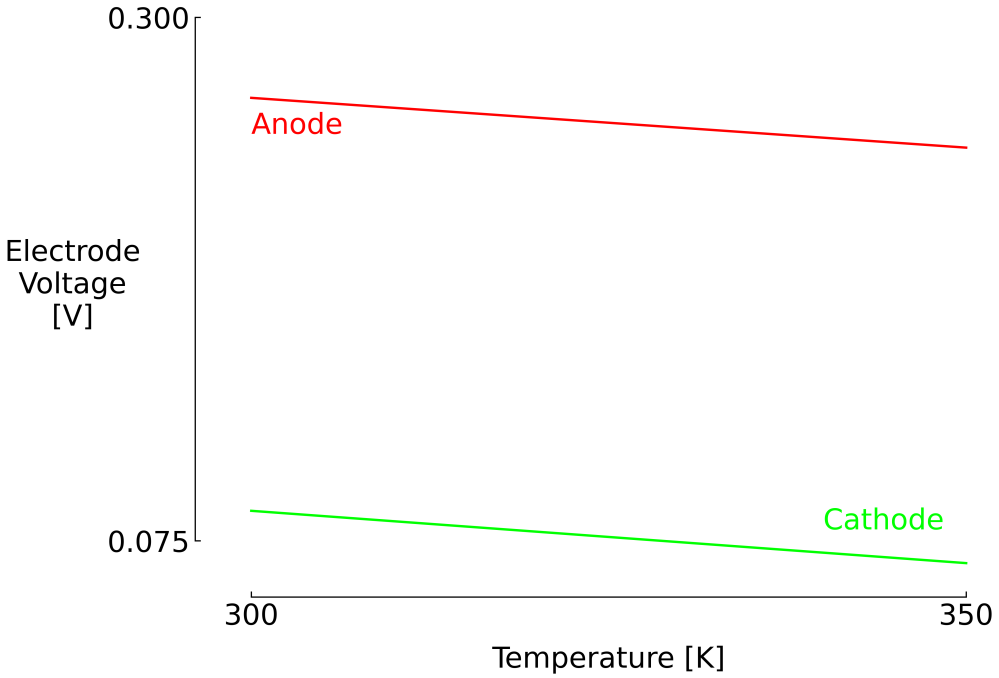

Figure 3.9: Evolution of the activation losses [V] according to the operating temperature [K] at the anode (red) and the cathode (green) for a constant current density

Ohmic losses

The ohmic losses are the consequence of the resistance encountered by the protons to cross the membrane. They are therefore directly linked to the properties of the material used and its dimensions. This resistance is characterised by the conductivity σ_M and the thickness δ_M of the membrane. The thickness remains of course constant, whereas the conductivity of the

material can vary according to the operating conditions. A semi-empirical expression 3.28 is therefore proposed [38].

$$\sigma = (0.005139\lambda - 0.00326)exp[1268\left(\frac{1}{303} - \frac{1}{T}\right)\ [S/m] \tag{3.28}$$

Where λ [-] is the excess water present in the membrane. In addition to the membrane we can also add the resistive effect of certain R_{other} components of the cell other than the membrane. The total ohmic losses therefore follow the following relationship 3.29.

$$E_{Ohm} = \frac{\delta_M}{\sigma_M} I + R_{other} \tag{3.29}$$

This expression is widely validated and used in the scientific literature to realistically represent the overall ohmic resistances. It is again interesting to know the evolution of these losses according to the evolution of the temperature. Again, according to figure 3.10, the increase reduces the ohmic losses and thus improves the performance.

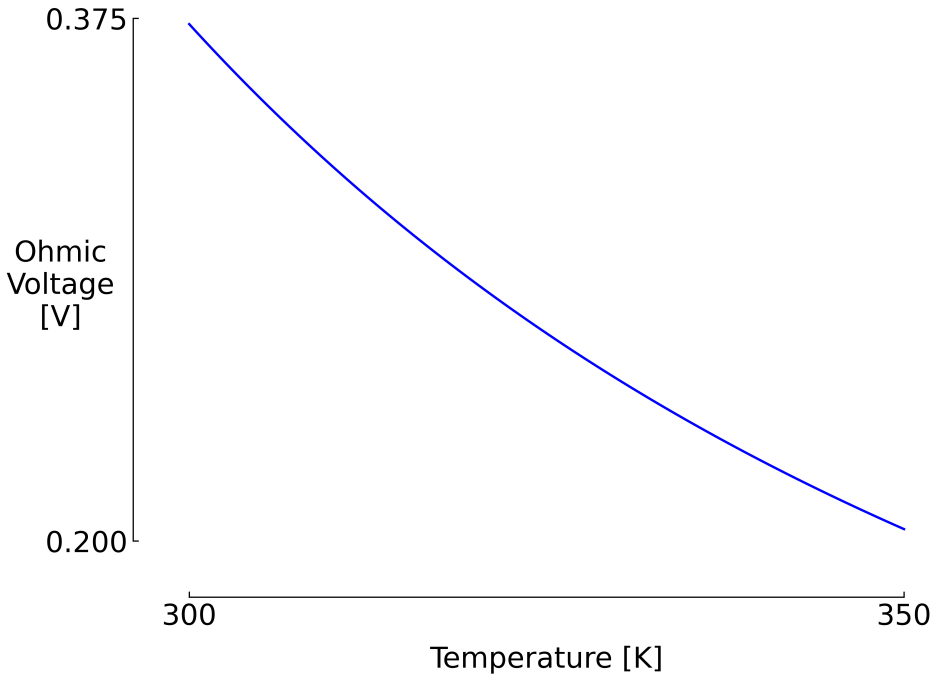

Figure 3.10: Evolution of the ohmic overpotential [V] according to the operating temperature [K] for a constant current density

Diffusion losses

The final overpotential that causes losses in the cell is mass transport. It occurs when the overpopulation of reactants on the surface of the electrodes prevents access to the reactants, leading to an increase in the potential required for the same current through the cell. This behavior is not observed untill relatively high current densities. This overpotential can be expressed simply by the maximum current density J_{lim} of the electrolyser [36].

$$E_{diff} = \frac{RT}{nF}\ \ln(1 - \frac{J}{J_{lim}}) \tag{3.30}$$

Above a certain current density, the mass transport losses become very important, reducing the cell efficiency [39]. It is therefore advisable to limit the load factor in order to maintain acceptable efficiencies.

Polarisation curve

As explained at the beginning of this section, the main objective of the electrical domain is to provide, on the basis of an input power, the corresponding current-voltage pair $(I - V)$. Indeed, the total potential of the cell, i.e. the reversible potential added to the various losses, is a function of the current density passing through the cell of the electrolyser. There is therefore a single operating point $I - V$ corresponding to the input power. As a first step, it seems interesting to observe the relationship between the current and the total potential of the cell. This relationship is more commonly known as the polarisation curve. It indicates, for a given temperature, all the potentials that need to be supplied to the cell as a function of the current density that we wish to have.

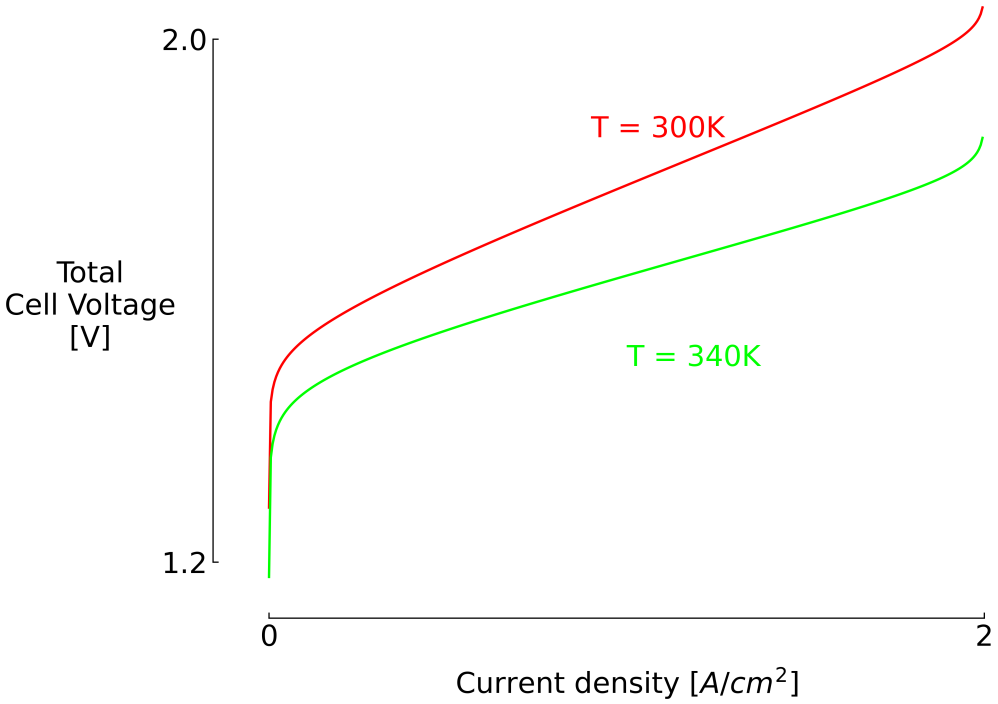

Figure 3.11: Polarisation curve of the electrolyser at 300 Kelvin (red curve) and 340 Kelvin (green curve)

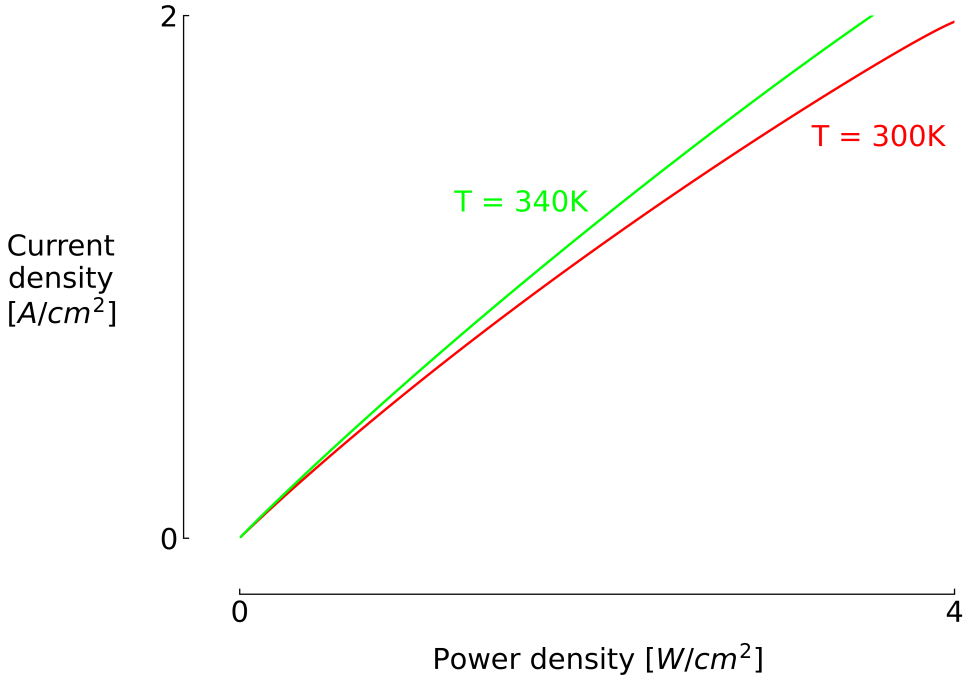

Figure 3.12: Evolution of the curent density [V] according to the power density input [W] at 300 Kelvin (red curve) and 340 Kelvin (green curve)

We should certainly not forget the impact that temperature has on this polarisation curve (Figure 3.11). All the observations on the previous sources of potentials are validated. When the operating temperature increases, the total potential of the cell decreases and this for the same current density. At high temperatures and for a given power, the cell allows more protons to pass. Based on the polarisation curve, it is also possible to obtain the link between the power density of the cell and the current density flowing through it (3.12) because the power is simply the product of the current and the voltage. In order to identify the current density corresponding to an input power, it is necessary to have a direct link between power and current. To this end, a three-dimensional polynomial fitting was performed between power, current density and temperature. For this purpose, we have to fit a third order polynomial between power and current density between a range of temperatures.

$$J(P,T) = a(T)P^3 + b(T)P^2 + c(T)P + d(T) \tag{3.31}$$

From this, the coefficients a, b, c and d are obtained, all of which are dependent on temperature. A second polynomial fitting of the second degree allows us to obtain the direct link between the coefficients and the temperature. If x represents each of the coefficients a, b, c or d, we obtain the following relationship:

$$x(T) = x_1\ T^2 + x_2\ T + x_3 \tag{3.32}$$

By substituting 3.32 for each coefficient in 3.31, we now have a direct relationship between the current density and the input power to the electrolyser. It is now possible to calculate precisely the different potentials presented on the basis of the current density and the operating temperature.

$$E_{cell}(J,T) = E_{rev}(T) + E_{act}(J,T) + E_{Ohm}(T) + E_{diff}(J,T) \tag{3.33}$$

The degrees of the polynomials were chosen to minimise the error between the true current density according to the power input and the current density based on the polynomial fitting.

$$Error = \frac{J_{True} - J_{Poly}}{J_{True}} \tag{3.34}$$

The polynomial fitting tends to underestimate the calculated current density compared to the real current density (Figure 3.13). However, the error observed remains less than 0.4% over the temperature range studied [300-350K] (Figure 3.14). It is therefore perfectly acceptable to use this method to calculate the current density corresponding to the input power at each time step.

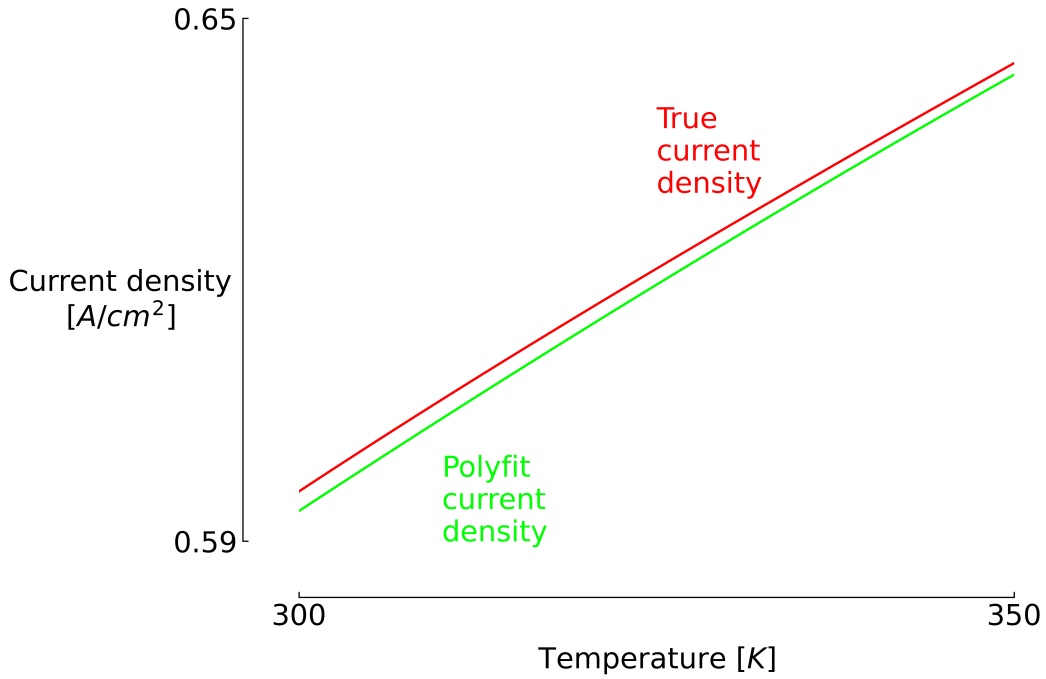

Figure 3.13: Evolution of the true current density and the polyfit current density according to temperature for a constant power density.

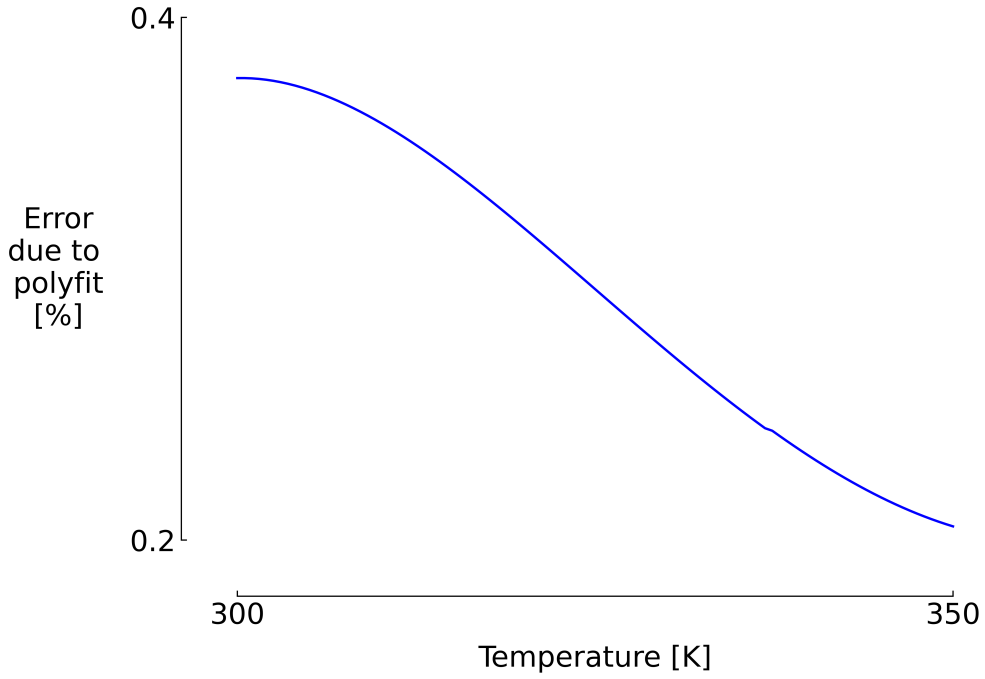

Figure 3.14: Evolution of the error [%] due to the polynomial fitting according to temperature for a constant power density.

Transient behavior of the electrical domain

All the potentials previously presented simulate the static behaviour of the cell. That is, so far no dynamics are taken into account. However, it has been observed that the activation potentials have a certain response time before reaching the voltage corresponding to the input power [41]. It is therefore interesting to integrate this dynamic behaviour into the model in order to analyse the impact it may have. Moreover, the system is powered by a very volatile power source, which encourages the study of this kind of dynamic phenomenon. As a first step, an equivalent circuit can be drawn with a capacitance across the activation potentials, where a response time is observed. This capacitance simulates the accumulation of charges at the edges of the electrodes which causes a delay in the dissipation of the charges (Figure 3.15).

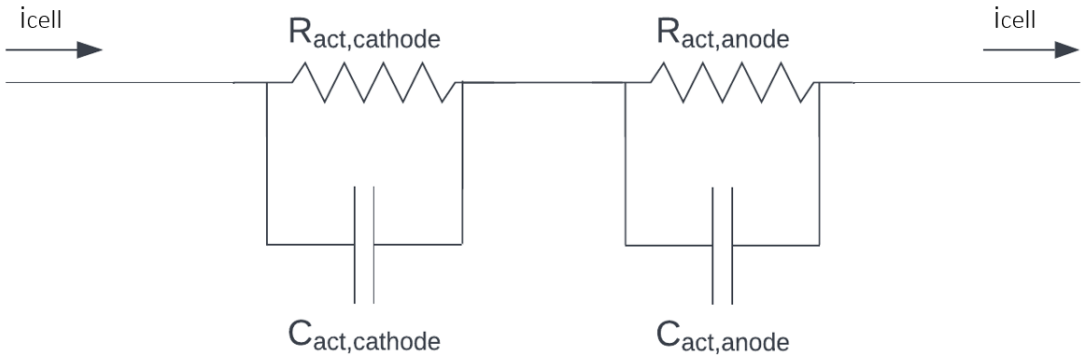

Figure 3.15: Equivalent circuit considering transient behavior for the activation overpotentials

The equivalent capacities at the anode and cathode can be quantified using the capacitance specific to the materials used and the geometry of the electrodes [42].

$$C_{act,i} = \frac{\epsilon A}{d}[F] \tag{3.35}$$

Where $\epsilon[F/m]$ is the electrical permittivity of the material, $A[m^2]$ is the area of the electrode and d is the distance between the two electrodes. The ratio $\frac{C}{A}$ has typical values as around $0.20F/m^2$ It remains now to know the resistances of the two electrodes [43]. Knowing the current flowing through them and the activation potential at each electrode, they are easily calculated.

$$R_{act,i} = \frac{E_{act,i}}{i_{cell}}[\Omega] \tag{3.36}$$

To visualise the evolution of this resistance, it is interesting to observe figure 3.16 where the equivalent resistance at the anode is computed.

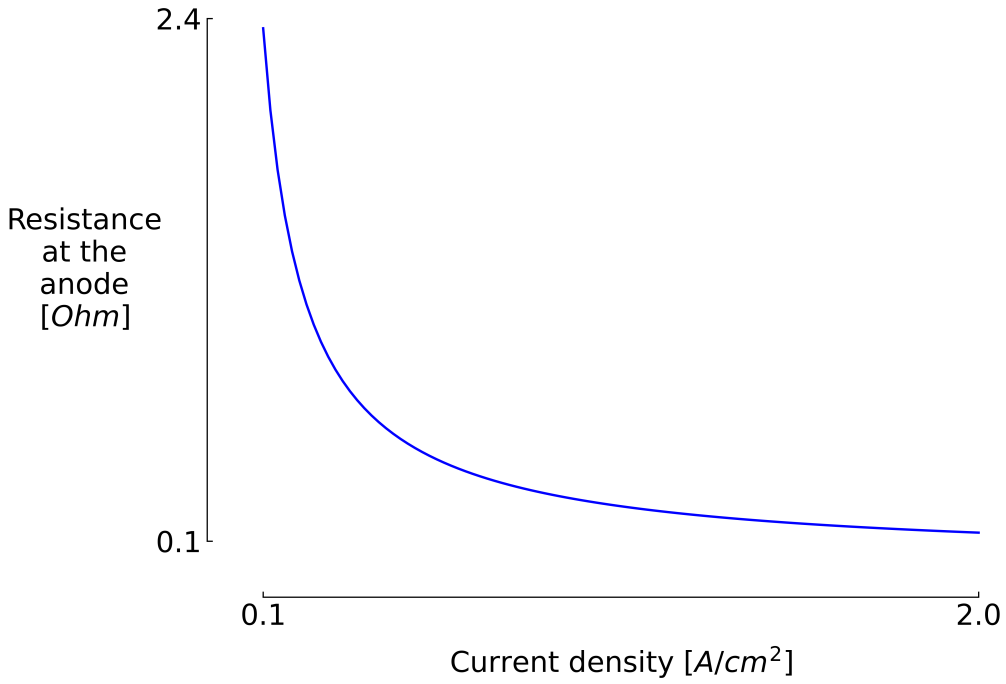

Figure 3.16: Evolution of the equivalent resistance at the anode according to the current density

When the current density is low, the resistance is high due to a large activation potential compared to the current density (Figure 3.17). Thereafter, the ratio of potential to current density keeps decreasing, which causes the equivalent resistance to drop. The same phenomenon can be observed at the cathode.

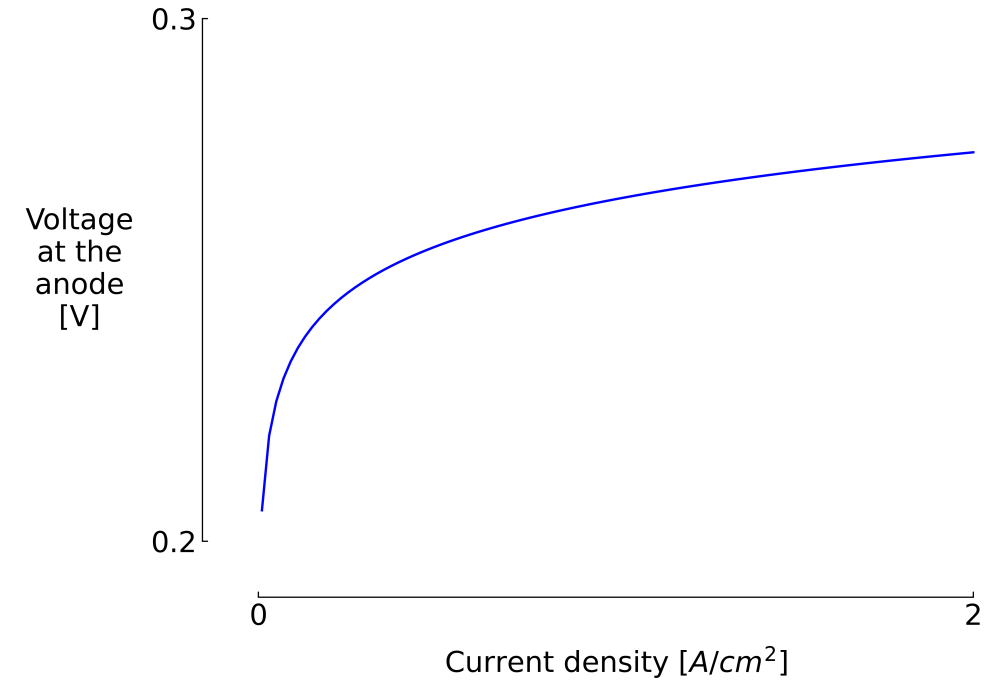

Figure 3.17: Evolution of the anode activation overpotential according to the current density

It is now possible to define the time constant (3.37) at each electrode with the known resitances and capacitance. The value of this time constant indicates the time it takes to

reach approximately 63% of the target voltage.

$$\tau_{act,i} = C_{act,i} R_{act,i} = C_{act,i} \frac{E_{act,i}}{i_{cell}} [s] \tag{3.37}$$

In view of the evolution of the resistance equivalent to figure 3.16, and this with a fixed capacity, it is clear that the time constant will be higher as the current density is lower. We can therefore already imagine that increasing the input power of the electrolyser will have the consequence of reducing its dynamic behaviour in the electrical domain. In order to integrate this time constant into the model it is necessary to express this dynamic behaviour by a differential equation 3.38.

$$\tau_{act,i} \frac{d(E_{act,i})}{dt} = E_{target,i} - E_{act,i} \tag{3.38}$$

Where $E_{target,i}$ is the target voltage, i.e. the expected voltage across the electrode in the case of a static model provided in the previous sections about the various overpotentials. This dynamic aspect of the electrical domain has the consequence of potentially decreasing the hydrogen production compared to a purely static model. Indeed, if the activation potential does not react quickly enough to a sudden increase in input power, then the supplied current is not fully used in the production of hydrogen. It is therefore necessary to recalculate the current corresponding to the real potential of the cell. To do this, it is sufficient to reuse the Butler-Volmer and Tafel law presented in equation 3.26 in the context of activation overpentials. By isolating the corresponding current density i we find :

$$i = i_0 \exp(\frac{E_{act,i} F \alpha_i z_i}{RT}) \tag{3.39}$$

It remains to be seen whether this dynamic behaviour has a significant impact on the performance of the electrolyser. A series of 20 simulations with a very volatile power profile shows the small impact that this dynamic aspect has on hydrogen production (Figure 1). The influence of the transient behaviour reduces the hydrogen production by a maximum of 0.04%. Beyond being very small, this impact will not be observable for higher time steps. It will therefore not be taken into account in the rest of this thesis in order to reduce the computational cost of the code as much as possible.

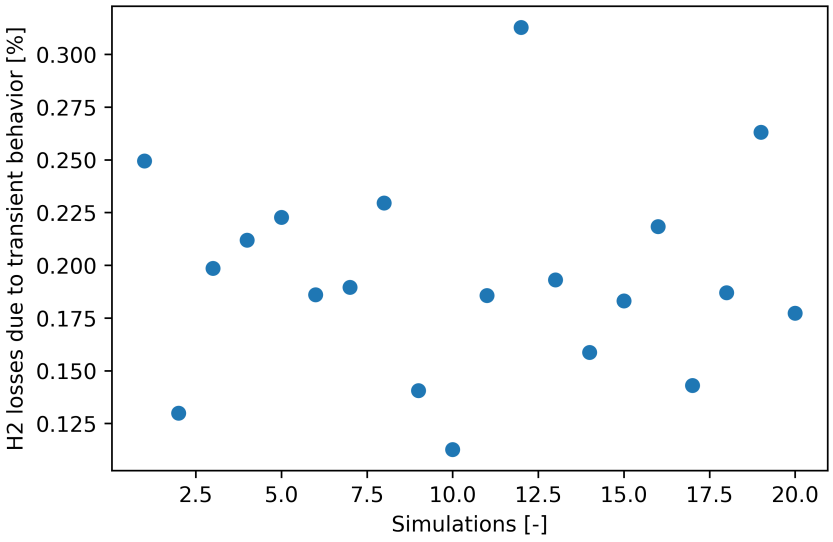

Figure 3.18: Hydrogen production losses ratio due to the transient behavior of the electrical domain for 20 aleatory simulations

Model validation

The electrolyser model has been validated on the basis of experimental data presented in the literature [44]. A real agreement is observed between the experimental data and the simulated curve. The values of the parameters used are available in table 5.3.

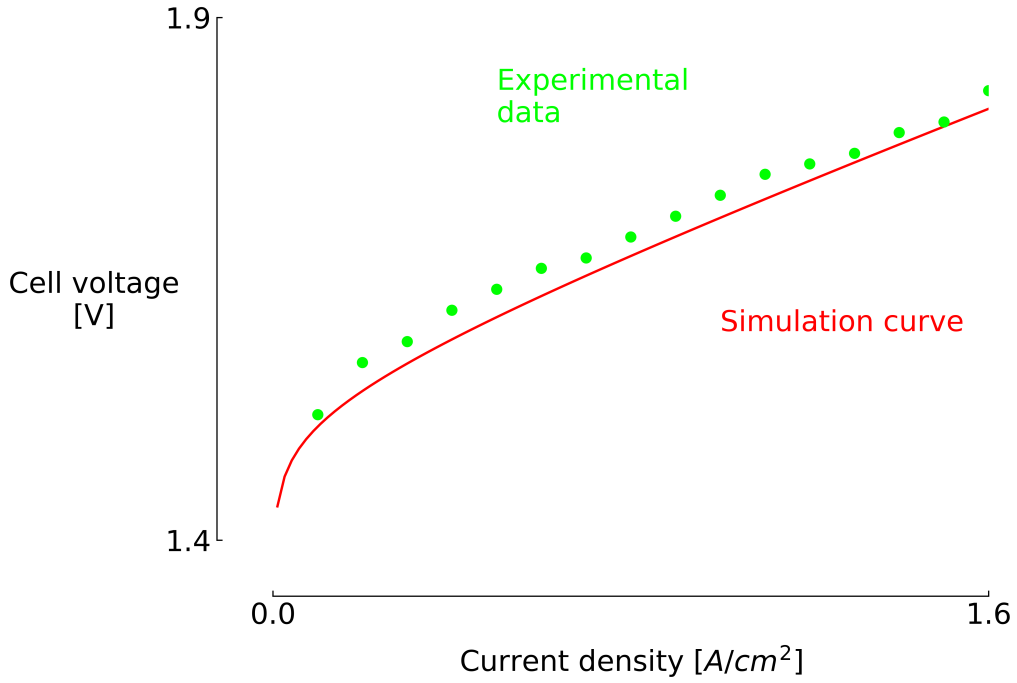

Figure 3.19: Validation of electrolyser model with experimental data of the cell polarisation curve at 80°C

3.3.2 Fluidic domain

The fluidic domain calculates all major molar flows within the cell. These include the hydrogen produced at the cathode, the oxygen produced at the anode and the water needed for the reaction. It is assumed that no flow crosses the membrane. The required water flow rate will be used later in the thermal domain. These molar flows are defined using Faraday's law.

$$H_2 = \frac{I\eta_F}{2F}\ [mol/s] \tag{3.40}$$

$$O_2 = \frac{I\eta_F}{4F}\ [mol/s] \tag{3.41}$$

$$H_2O = \frac{I\eta_F}{2F}\ [mol/s] \tag{3.42}$$

Where I is the current through the electrodes and η_F is the Faraday efficiency. This efficiency is measured by the ratio of the actual hydrogen flow to the theoretical hydrogen flow. These losses are caused by parasitic currents. In reality, this Faraday efficiency is usually measured as being greater than 99% and is therefore neglected in this thesis.

3.3.3 Thermal domain

As observed for the electrical domain, the operating temperature has a significant impact on the overall performance of the electrolyser. Moreover, knowing the inertial character of the

temperature, it is essential to provide the electrical domain with a temperature according to a dynamic model, and not a static one, in order to obtain realistic results. A homogeneous temperature within the cell is assumed to avoid the need to differentiate temperatures according to the position in the cell, which would imply a high computational cost. The thermal domain of the electrolyser therefore aims at knowing the evolution of the operating temperature within the cell at any time time step. The first thing to do is to identify the main sources of heat present in the electrolyser. The first is the heat input resulting from the electrical potential in the cell [45].

$$Q_{elec} = (E_{cell} - E_{tn})\ J\ A\ [W] \tag{3.43}$$

Where E_{tn} is the thermoneutral voltage, as presented in equation 3.22, and A the surface area of the membrane. When the total electrical potential of the cell is greater than this thermoneutral voltage, the heat input is positive and tends to raise the temperature within the cell. It is this heat flow that allows high temperatures to be reached, improving performance. However, an extreme high temperature can damage the proton exchange membrane. Fortunately, there is a second heat flow to counterbalance this. Indeed, the electrolysis reaction requires an abundant amount of water to ensure a complete reaction. When this water passes through the cell, it absorbs a certain amount of heat according to the following expression.

$$Q_{water} = (T_{water} - T_{cell})\ c_{p,water}\ \dot{m}_{water}\ [W] \tag{3.44}$$

Where T_{water} is the temperature of the water, this temperature is assumed to be constant during a simulation where $c_{p,water}$ is the specific heat of the water and $\dot{m}_{water}$ is the water flow rate through the cell. In order to know the water flow rate at each time step, it is preferable to use the excess water symbolised by λ. For a certain current through the cell, as treated in the fluidic domain, corresponds a minimum flow of water to ensure a complete reaction at the cathode. This minimum flow rate is theoretical, because in practice, if one sticks to this flow rate, it is impossible to make it react completely. It is therefore necessary to increase this flow rate for two main reasons. The first is the one mentioned above. The second is the need to maintain a sufficient flow rate to ensure that the products of the reaction are removed from the cathode. The excess water is finally expressed according to the equation 3.45

$$\lambda = \frac{\dot{m}_{water}}{\dot{m}_{theo}} = \frac{\dot{m}_{water}}{M_{m,H_2O} I/2F}\ [-] \tag{3.45}$$

The heat flow related to the passage of water can therefore be rewritten by taking the excess water coefficient into consideration.

$$Q_{water} = (T_{water} - T_{cell})\ c_{p,water}\ \lambda * \frac{M_{m,H_2O} I}{2F}\ [W] \tag{3.46}$$

There is one last heat flow to be taken into account, and that is the heat exchange between the external environment and the cell of the electrolyser. This flow depends largely on the atmospheric conditions surrounding the installation and the thermal resistance R_{th} of the cell. The equation 3.47 brings these parameters together to express the heat exchange with the surrounding environment.

$$Q_{amb} = (T_{amb} - T_{cell})\ \frac{1}{R_{th}}\ [W] \tag{3.47}$$

Now that all the heat flows have been correctly expressed, it is possible to give the temperature within the cell as a function of them. To do this, it is necessary to know the thermal

capacitance of the electrolyser C_{th}, i.e. the number of joules that it is necessary to supply to the system in order to increase its temperature by one. This leads to a differential equation 3.49.

$$C_{th}\frac{dT_{cell}}{dt} = Q_{elec} + Q_{water} + Q_{amb}\ [W] \tag{3.48}$$

In which all heat flows are known. Replacing them allows to visualise the differential equation with the temperature in the cell as the only variable [45].

$$C_{th}\frac{dT_{cell}}{dt} = (E_{cell} - E_{tn})\ J\ A + (T_{water} - T_{cell}) * c_{p,water}\ \lambda\ \frac{M_{m,H_2O}I}{2F} + (T_{amb} - T_{cell})\ \frac{1}{R_{th}} \tag{3.49}$$

The figure 3.20 shows an example of the evolution of the different heat fluxes present in the cell of the electrolyser for a random power profile with a time step of one minute. It can be seen that it is mainly the negative heat flux of the water that compensates for the heat brought by the electrical potentials in the cell. The ambient temperature, for a relatively well thermally insulated cell, has little impact on the temperature evolution.

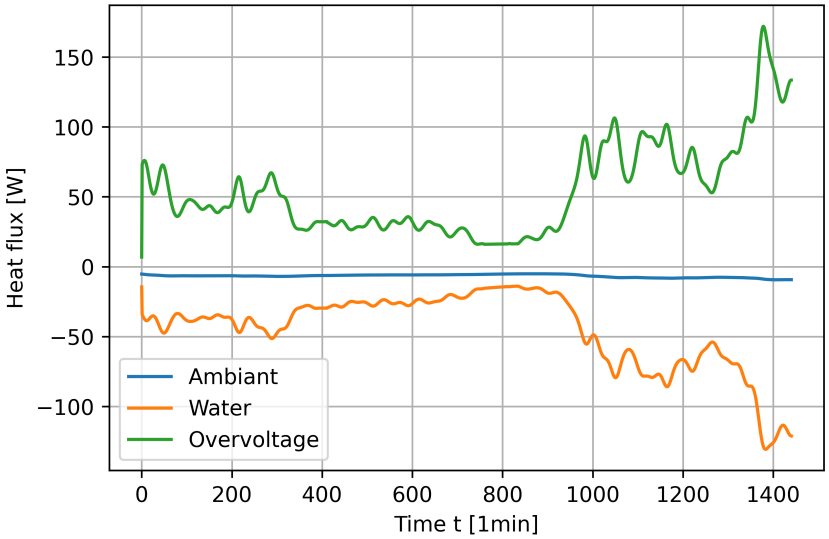

Figure 3.20: Evolution of the different heat fluxes in the cell responsible of the temperature evolution

As it was done for the transient behavior of the electrical domain, it is interesting to know the impact that the dynamic thermal model can have on the hydrogen production of the electrolyser. To do this, the temperature evolution between a static and dynamic model is compared for an identical scenario (Figure 3.22). The dynamic model implies serious temperature variations. It therefore seems necessary to opt for a model that considers the dynamism of the temperature. The error in terms of hydrogen production is obvious. The static model has an error of up to 4% compared to the hydrogen production rate of the dynamic model. Given the influence of temperature on the performance of the system, it is necessary to include this dynamic behaviour for maximum accuracy.

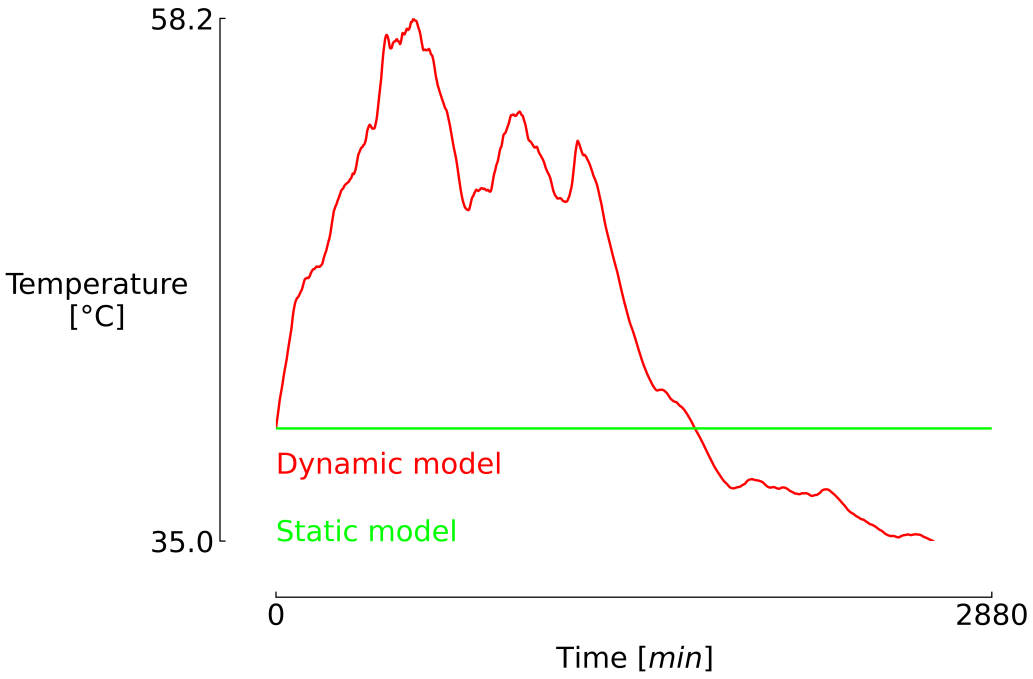

Figure 3.21: Evolution of the temperature in the cell for a dynamic model compare to the static model

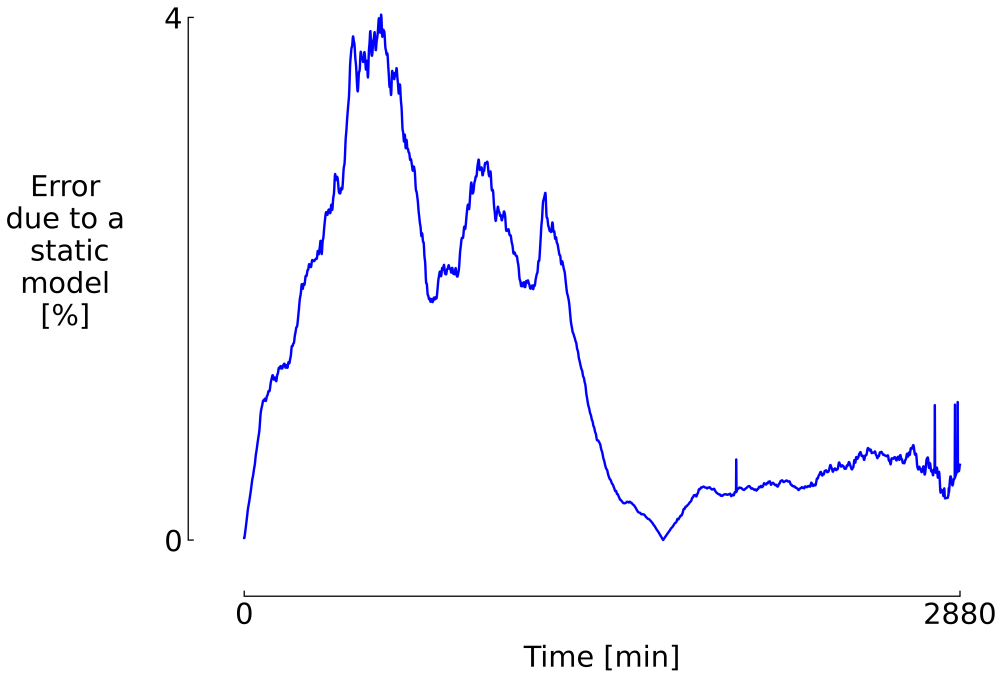

Figure 3.22: Error made by the static model in terms of hydrogen production rate

3.3.4 Domains connections

Based on the previous sections, there are clear connections between each of the three domains presented. The diagram in figure 3.23 shows these interactions more easily. The electrical domain provides the current density, based on an input power, to the fluid domain which in turn can provide the water flow to the thermal domain. The latter also receives information

on the current density and the total potential of the cell from the electrical domain with which it can determine the temperature evolution. Finally the temperature is sent to the electrical domain and the loop is closed.

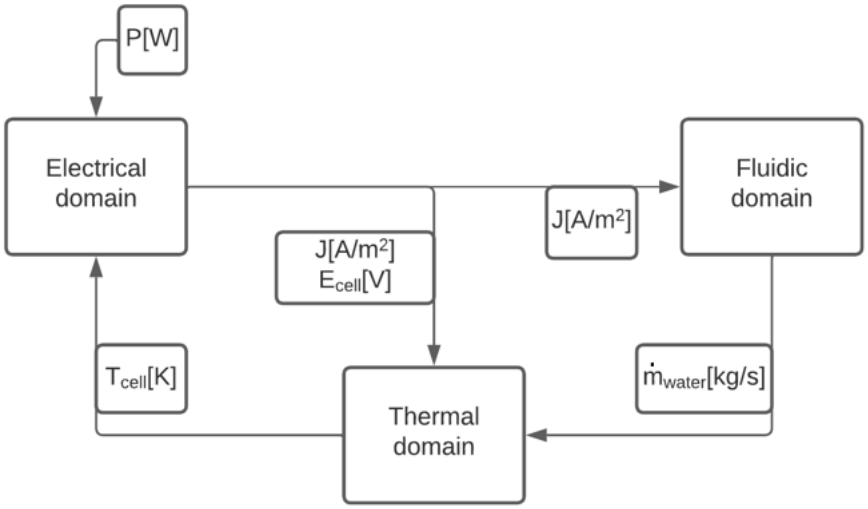

Figure 3.23: Connection between the three domains used in the code

3.3.5 Cell efficiency

As explained in the previous sections, the separation of water into oxygen and hydrogen protons requires a certain amount of energy. This energy takes the form of electrical potential in the case of the electrolyser. In addition to this potential directly related to the separation of water, there are electrical overpotentials leading to energy loss. The efficiency can therefore be translated as the ratio of the energy produced via hydrogen gas production to the energy supplied in the form of electrical potential and current. In order to quantify the energy produced in the form of hydrogen, it is possible to use its lower heating value (LHV) or its higher heating value (HHV). In general, HHV is preferred to LHV in liquid water electrolysis. The electrical efficiency of the electrolyser cell is finally defined by the equation 3.50.

$$\eta_{elec} = \frac{HHV * \dot{m}_{H2}}{P_{elec}} = \frac{HHV * \dot{m}_{H2}}{E_{cell} * I_{cell}} \tag{3.50}$$

This efficiency can be expressed solely with the help of the current and voltage data using the equations 3.23 and 3.40. The latter provides the molar flow rate of hydrogen produced, which must be multiplied by the molar mass of water to obtain a mass flow rate. The efficiency can be rewritten:

$$\eta_{elec} = \frac{HHV * \frac{I_{cell}\eta_F}{2F} * M_{m,H_2O}}{(E_{rev} + E_{act} + E_{diff} + E_{Ohm}) * I_{cell}} = \frac{HHV * \frac{\eta_F}{2F} * M_{m,H_2O}}{(E_{rev} + E_{act} + E_{diff} + E_{Ohm})} \tag{3.51}$$

This efficiency in this case does not represent the overall efficiency within the cell. Indeed, as presented previously, electrolysis is an endothermic reaction requiring a heat input. This heat input is translated by the thermoneutral voltage 3.22. In general, heat is supplied by the cell potential when it is higher than the thermoneutral voltage. At very low current densities it may be lower and it is therefore necessary to supply heat to the cell by some other means.

This lack of energy can be translate through an electrical potential via the thermoneutral voltage and the cell voltage [46].

$$E_{lack} = max(E_{tn} - E_{cell}, 0) \tag{3.52}$$

This necessary energy must be added to the efficiency to obtain the overall efficiency of the cell.

$$\eta_{cell} = \frac{HHV * \frac{\eta_F}{2F} * M_{m,H_2O}}{(E_{rev} + E_{act} + E_{diff} + E_{Ohm} + E_{lack})} \tag{3.53}$$

It is now possible for the model to calculate the efficiency of the reaction based solely on the electrical potentials. The figure 3.24 shows the evolution of this efficiency as a function of the current density for two different operating temperatures. The impact of temperature is again evident, a higher temperature undeniably improves the efficiency of the cell.

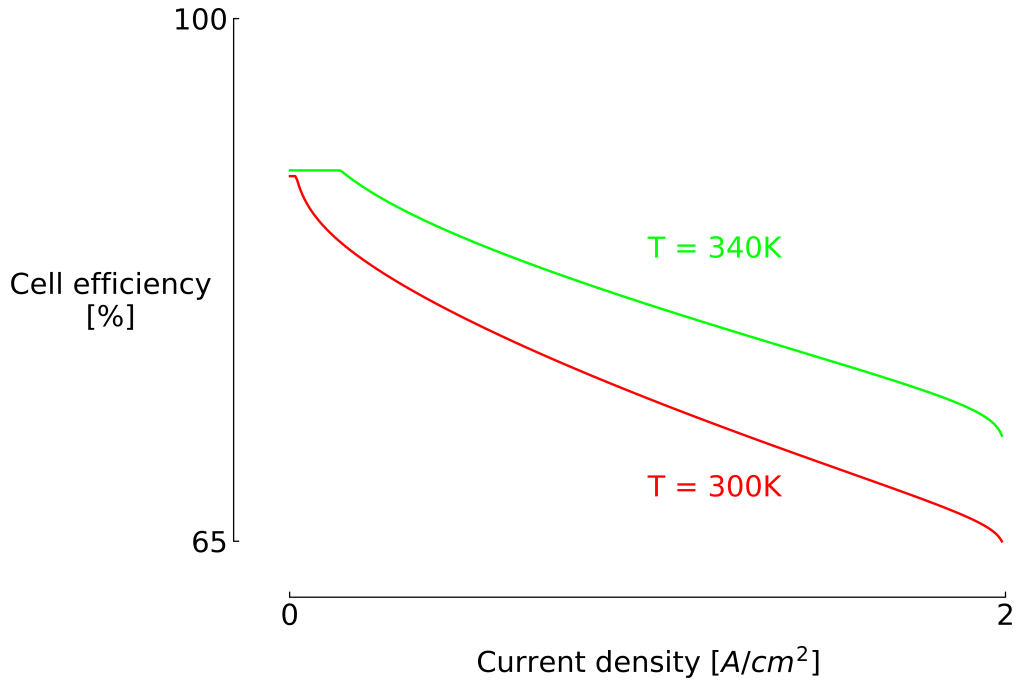

Figure 3.24: Evolution of the cell efficiency $[\%]$ according to the current density $[A/cm^2]$ at 300 Kelvin (red curve) and 340 Kelvin (blue curve)

The analysis of the overall efficiency of the electrolyser has shown that a rather limited operating range is available if one wishes to optimise hydrogen production. Indeed, at high load, the the overpotentials increase a lot and thus reduce the cell efficiency. The system is therefore faced with a problem because the power source is extremely volatile, making it impossible, at first sight, to operate within a limited range. In order to overcome this problem, it was decided to integrate batteries into the model to buffer these extreme production zones. The following section presents the battery model used.

3.4 Battery model

As the battery is not the main focus of this thesis, a simplified static model has been preferred to a complex dynamic model. It is based on lithium batteries for which the transition from charge to discharge can realistically be assumed to be instantaneous [47]. The main

parameters are the maximum capacity Q_{max} and the discharge efficiency η_d and charge efficiency η_c of the battery [48]. The state of charge soc is also required:

$$soc = \frac{Q_{bat}}{Qmax} \tag{3.54}$$

Where Q_{bat} is the energy stored in the battery. The evolution of this state of charge depends entirely on the charging power L_c and discharging power L_d of the battery. During the simulation, this state of charge is constantly calculated in order to manage the use of the battery.

$$\frac{d(soc)}{dt} = L_c - L_d = P_{in} * \eta_d - L_d \tag{3.55}$$

Where P_{min} is the input power of the battery to which of course the charge efficiency must be added to obtain the net power.

3.5 Grid model

The grid is modelled as simply as possible. When additional power is required due to depleted batteries, the grid responds directly. The energy supplied by the grid to the system is recorded at the end of each simulation in order to reduce its dependence to a minimum. This dependency is defined as the share of energy purchased from the grid relative to the share of energy supplied by the wind farm.

$$\eta_{grid} = \frac{\sum P_{grid}}{\sum P_{WF} + \sum P_{grid}} \tag{3.56}$$

In the interest of making the system as independent as possible, it is necessarily desirable to reduce this part of the grid to a minimum.

Chapter 4

Methodology

This chapter presents the methodology used to obtain the results. First, the system objectives are detailed. These are sensitive to the uncertainty related to the wind speed at the wind turbine. The idea is to know how the system design variables can influence the sensitivity of the objectives when they are subject to uncertainty. A deterministic optimisation is thus first performed to identify several designs that favour the objectives in different ways. Finally, uncertainty is propagated through these designs to find out the sensitivity of the objectives.

4.1 Objectives

The main objective is to know how to increase the flexibility of the system. In this case, the modelled system is used to store intermittent energy produced by a wind farm. Flexibility can therefore be defined as the ability of the system to adapt to the electricity production. PEM technology was initially chosen for its capacity to react to the volatility of its input power. However, the intermittency of the wind speeds forces the electrolyser to reach too high current densities where the efficiency is very low. In addition, this constant dynamic regime within a cell causes significant degradation which greatly reduces its life span. In order to address these issues, batteries have been added to the system to study the impact they may have. The overall objective is to ensure that the system recovers most of the energy produced by the wind farm while limiting the degradation of its components.

4.1.1 Objective 1 : share of grid and losses

A high degree of autonomy demonstrates the flexibility of the system, i.e. the ability to adapt to major fluctuations on its own. Therefore, the first objective is to minimise the share of energy supplied by the electricity grid in the system. In addition, it is desirable to also minimize the losses incurred when the batteries are fully charged. In order to simplify the process these two objectives have been combined into one. Minimising the sum of the energy supplied by the grid plus the losses in relation to the total power supplied to the system (wind farm + grid) becomes the first objective.

$$Obj_1 = min(\frac{\sum P_{grid} + E_{loss}}{\sum P_{WF} + \sum P_{grid}}) \tag{4.1}$$

4.1.2 Objective 2 : lifetime of the electrolyser

To study the flexibility of a power to hydrogen system, it is necessary to understand the evolution of the degradation of the system components. In this case, for the electrolyser,

there are two main sources of performance loss. These must be differentiated between dynamic and stationary operating conditions [50]. The degradation under static conditions is completely resorbed during a variation of intensity within the electrolyser. Indeed, it has been observed that the degradation accumulated during a static regime is completely recovered after the interruption or the variation of the current. For this reason, the temporary degradation under static regime has not been taken into account in this model. It remains to be seen how the degradation under dynamic operating conditions evolves. A first cause is the kinetic deactivation, resulting from a contamination of the anode by Titanium (Ti) [51]. This Ti comes from Titanium dioxide $Ti0_2$, itself present in the catalyst. The second phenomenon is the increase of the resistivity of the membrane when the current intensity varies, causing a degradation of the PEM membrane. The performance losses described above under dynamic regime are permanent. Therefore, it is necessary to quantify these losses within the system. First of all, it is important to identify when the system enters a dynamic regime, i.e. when the input power of the electrolyser undergoes variations. To do this, the time derivative of the ohmic overpotential of the membrane is constantly analyzed by the model to detect some variations.

$$dyn = \frac{d(E_{Ohm})}{dt} \tag{4.2}$$

When dyn is different from 0, the electrolyser enters a dynamic regime (Figure 4.1).

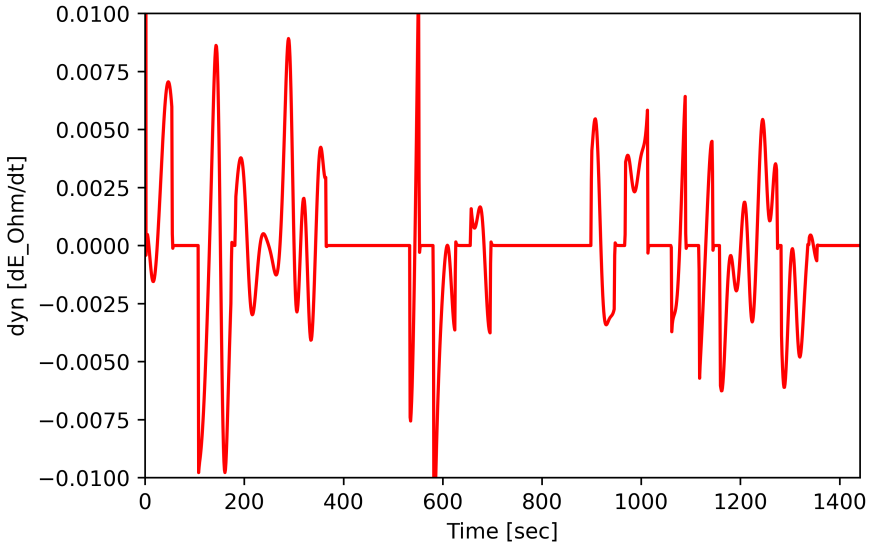

Figure 4.1: Detection of dynamic regime in the cell through the dyn variable

The degradation is generally characterized by an increase in voltage, expressed in $[\mu V/h]$, and a decrease in current density, expressed in $[\mu A/cm^2/h]$. Georgios Papakonstantinou et al [51] expect a degradation of $35.2\mu V/h$ under dynamic conditions. In the dynamic regime, the model stores the accumulation of these degradations in two variables ($degrad_J$ and $degrad_E$) and adds them at each time step to the total cell voltage E_{cell} and the current density J_{cell}.

$$E_{cell,degrad} = E_{cell} + degrad_E \tag{4.3}$$

$$J_{cell,degrad} = J_{cell} - degrad_J \tag{4.4}$$

The consequence of this degradation is a loss of performance of the electrolyser. For the same power input to the cell, the electrical potential required is now higher and this for a lower current density. The relationship 3.40 confirms that a smaller quantity of hydrogen

will then be produced by the electrolyser, resulting in a drop in efficiency. It is through this relationship that the life of the electrolyser is estimated. When the decrease in efficiency, for the same load factor, is considered too high, the electrolyser is considered to be at the end of its life.

$$\eta_{loss} = \frac{HHV * \frac{\eta_F}{2F} * M_{m,H_2O}}{E_{cell}} - \frac{HHV * \frac{\eta_F}{2F} * M_{m,H_2O}}{E_{cell,degrad}} \tag{4.5}$$

This permitted efficiency loss limit has to be defined by the user. The equation 4.5 is used to find the maximum permitted degradation in terms of voltage ($degrad_{E,max}$). In general we accept a degradation of 2% [51]. With the total degradation recorded at the end of the simulation ($degrad_{E,sim}$) over a certain period of time T, the lifetime of the electrolyser is defined as such:

$$LF = T\frac{degrad_{E,max}}{degrad_{E,sim}}\ [years] \tag{4.6}$$

This lifetime is based solely on the degradation associated with dynamic operations. According to this model, an electrolyser operating at constant load would have an infinite lifetime. This is of course not the case as other degradations independent of the operating regime occur. However, these degradations are still poorly documented in the literature, so it was preferred to use only the available data considering that the obtained lifetimes are a good way to study the impact of dynamic operations on the electrolyser. The lifetime of the electrolysers is therefore the second objective.

$$Obj_2 = min(LF_{PEM}) \tag{4.7}$$

4.1.3 Objective 3 : lifetime of the battery

The battery is also subject to varying degrees of degradation. It is therefore desirable to ensure that this degradation is minimised to give the system the longest possible lifetime. In the first instance, since an extreme state of charge will cause considerable damage to the battery, it is limited to between 10 and 90

$$10\% < soc < 90\% \tag{4.8}$$

Then, in order to quantify the degradation of the battery, it is necessary to know the number of cycles performed in relation to its maximum capacity. This is done by summing the total number of charges and discharges during the simulation.

$$n_{cycles} = \frac{\sum(L_d + L_c)}{2Q_{max}} \tag{4.9}$$

A factor of two is used in the denominator because a full cycle corresponds to a complete discharge and charge of the battery. By considering a maximum number of cycles equivalent to the end of life of the battery, the theoretical lifetime LT can be interpolated.

$$LT = T\frac{n_{max}}{n_{cycles}}\ [years] \tag{4.10}$$

Where T is the period over which the simulation was performed and n_{max} is the maximum number of charge cycles the battery can perform. This lifetime will be optimised in order to maximize the lifetime of the system taking into account the degradation of the electrolyser presented above.

$$Obj_3 = min(LF_{bat}) \tag{4.11}$$

4.2 Simulation example

This section presents the general operation of the model based on a random design. This allows the reader to correctly identify the impact that system variables may have on the functioning of the system and the data collected.

4.2.1 Power profile

The power profile simulated by the stochastic process takes place over a period of 30 days with a time step of ten minutes. It was decided to carry out the simulations over a period of one month in order to explore all possible operating conditions of the system. Indeed, a period that is too short sometimes prevents the observation of certain phenomena due to a power profile that is not extreme enough. Figure 4.2 shows a typical profile simulated by the stochastic process for both this example and the results.

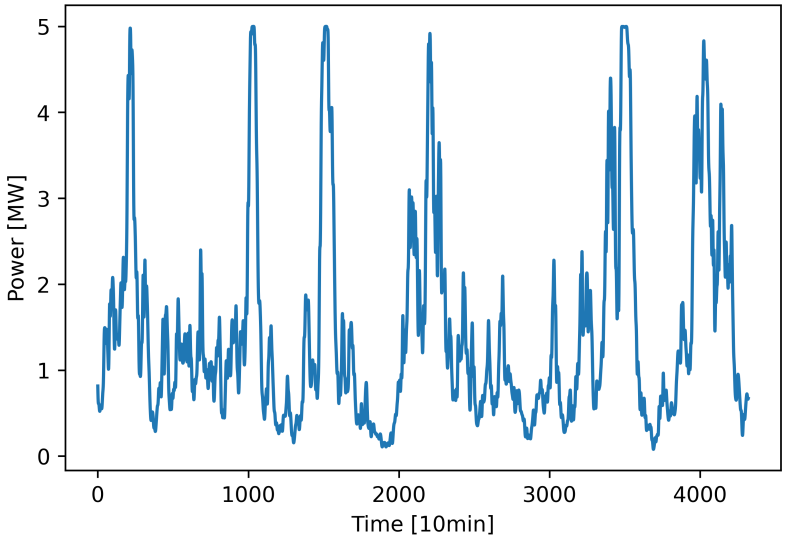

Figure 4.2: Typical power profile used

This is the power generated by the wind field sent directly to the electrolyser/battery system. The latter reacts differently depending on its design variables.

4.2.2 Design variables

This model has two main design variables. The first is the minimum current density allowed in the electrolyser. It therefore determines when the missing energy must be supplied from the batteries or from the grid. In this example the variable is set to :

$$J_{min} = 0.9[Acm^{-2}] \tag{4.12}$$

Knowing that the limiting current density J_{lim} in the electrolyser is $2[Acm^{-2}]$, the electrolyser operates only in the interval $[0.9; 2][Acm^{-2}]$. Ces limites de densités de courant sont ensuite traduites en puissances.

The second variable determines the number of electrolyser cells used to meet the power profile. In reality, this variable is determined by the maximum virtual current density per cell

$J_{peak,cell}$. In other words, the maximum current density per cell in case the batteries are not used and the electrolyser accepts all the power supplied by the wind field. This variable is first converted into the maximum power per cell by the polynomial fitting presented earlier. Then, this power is translated into a number of cells in relation to the maximum power generated by the power profile of the wind farm.

$$n_{cell} = \frac{P_{max,WF}}{P_{peak,cell}(J_{peak,cell})} \tag{4.13}$$

The choice of using this variable in terms of current density rather than in terms of power is justified by the desire to keep the variables independent of the system design.

It is also possible to change some other system parameters such as the maximum battery storage capacity per electrolyser. However, this has been kept fixed at $10kWh$ per electrolyser cell. This value was determined on the basis of a complete discharge in about 20 hours.

4.2.3 Outputs

When all variables are determined the simulation can start. For information, this requires a calculation time of about ten seconds per thousand time steps. The simulation over one month therefore requires about 40 seconds for a time step of ten minutes.

The first interesting data to be received are the powers at different levels of the system. Figure 4.3 shows the evolution of the power generated per cell unit and the power actually accepted by the cell. The upper and lower plateaus are clearly visible and represent the extreme powers allowed in the electrolyser. As can be seen in the figure 4.4, above the upper level the batteries are discharged while below the lower levels the batteries are discharged. When the batteries are empty, the electrical network is requisitioned to avoid the cut-off of the electrolyser. The total energy supplied by the grid is calculated at the end of the simulation to find the dependency of the system on the grid.

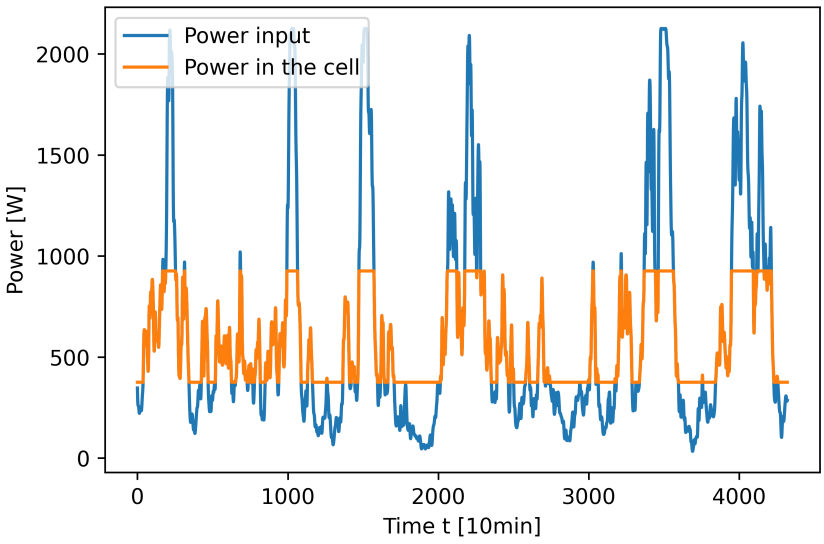

Figure 4.3: Power generated per cell unit in blue and power allowed in the cell in orange

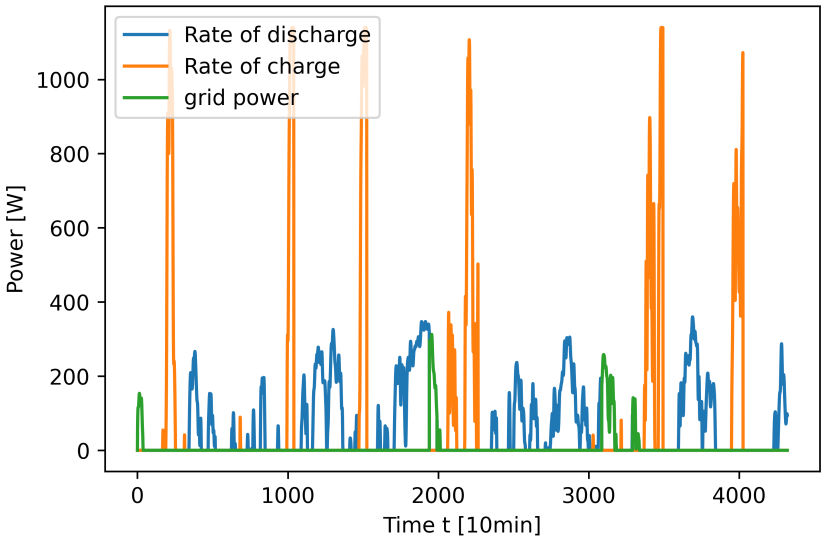

Figure 4.4: Charge (orange) and discharge (Blue) power of the battery and grid power in green.

The life of the battery is calculated using the number of complete cycles achieved by the battery (Figure 4.5). The state of charge presented is between 10 and 90% in order to limit the degradation of the battery as much as possible. Finally, the lifetime of the electrolyser is calculated by accumulating the degradation during the dynamic regimes (Figure 4.6).

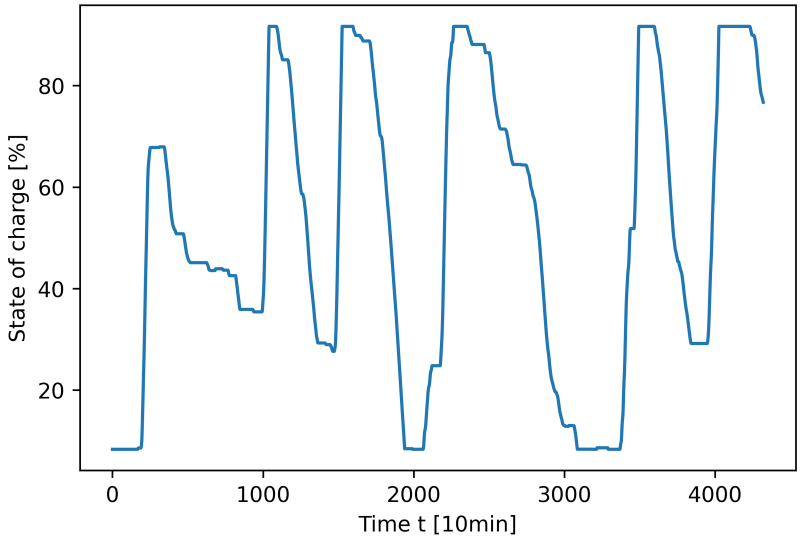

Figure 4.5: Evolution of the state of charge of batteries

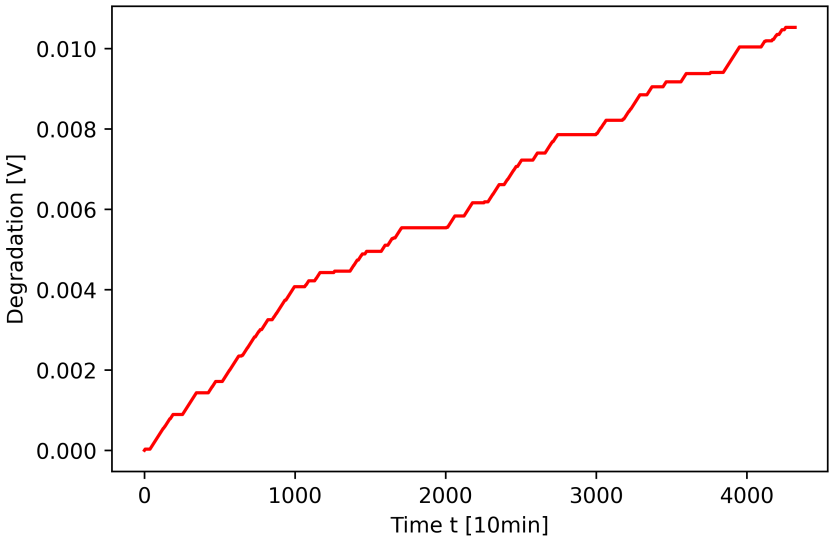

Figure 4.6: Cumulative degradation of the PEM electrolyser expressed in Volt

4.3 Deterministic optimisation

With the objectives clearly defined, the first step is the deterministic optimisation of the system through the design variables. "Deterministic" indicates that no stochasticity is present in the system parameters. For this purpose, the second version of the Nondominated Sorting Genetic Algorithm (NSGA-II), developed by Deb et al, is used [49].

4.3.1 NSGA-II - Optimisation method

NSGA-II is a genetic algorithm suitable for complex and non-linear models [49]. Initially a parent population P_0 is generated based on a Design of Experiment (DoE) scheme. This scheme is a Latin Hypercube Sampling in the RHEIA framework used. The NSGA-II algorithm then optimises the objectives using an iterative process. To understand this process, it is important to identify the three major mechanisms.

Non-dominated sorting procedure

The purpose of this mechanism is to sort each sample p_i of the population Rt of solutions according to their dominance over the other samples. Two variables allow this sorting, the number of solutions dominated by p and the number of solutions that dominate p. If the sample p is non-dominated it is placed in the list F_1. If it is dominated by only one other solution it is then placed in the list F_2 and so on. When the sorting is complete, the algorithm ideally keeps only the most dominant half of the starting population Rt. However, when there is a list F_i straddling the two halves, it is impossible for the non-dominated sorting mechanism to sort the samples in this list. Another process is then required.

Crowding distance sorting

This mechanism aims to ensure the diversity of the population by calculating the crowding distance of each sample p. This distance corresponds to the cuboid formed by connecting the two solutions adjacent to p with parallel segments. The solutions with the smallest crowding

distances are then located in a region dense with samples. These are then eliminated in priority from the F_i list. Of the population Rt only the next parent population P remains.

Next population generation

The final step is to create an offspring generation Q of the same size as the population P by mutation and crossover methods. The cycle is then repeated according to the number of generations allowed by the user.

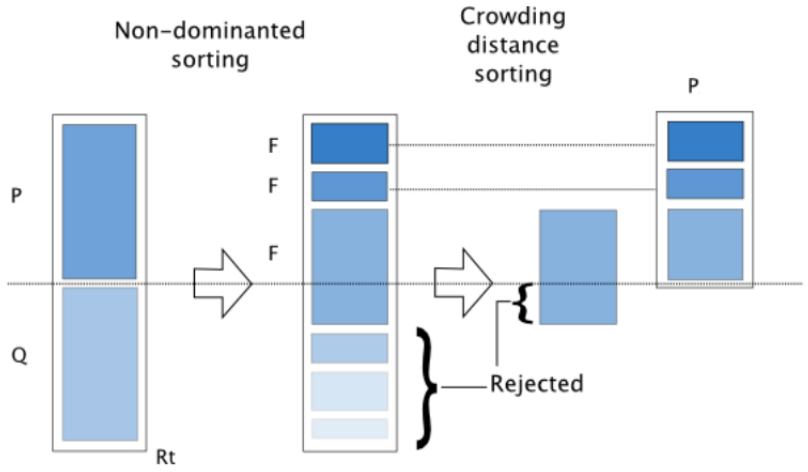

Figure 4.7: NSGA-II genetic optimisation loop from [52]

4.4 Uncertainty quantification

After optimising the system on the basis of the different input variables, it is possible to perform a sensitivity analysis on the objectives of interest. The algorithm used for this uncertainty quantification is the Polynomial Chaos Expansion (PCE), presented in this section. The objective of this process is to quantify the variability of the system's performance [53]. To do this, some parameters are characterised by a stochasticity that can be observed in reality. This stochasticity has two main origins. It can be due to the purely random character of certain data (wind speed) or linked to the imprecision following the lack of information (thermal resistance of the cell). They are respectively named as random and epistemic uncertainties. They are characterised by normal and/or uniform distributions in the PCE algorithm.

4.4.1 Polynomial Chaos expansion

In view of the cost of calculating the model, using Monte Carlo to calculate the uncertainties would be too time-consuming. This is why the model is tuned using an surrogate model which in turn allows Monte Carlo to be applied. The surrogate model in question is therefore in our case the PCE. The latter is constructed using orthogonal polynomials such as the Legendre polynomial for Unifor distributions and the Hermite polynomial for Gaussian distributions. Two factors determine the number $P+1$ of truncated series, the degree p of the polynomial and the dimension d of the stochastic space.

$$P + 1 = \frac{(p+d)!}{p!d!} \tag{4.14}$$

As a result, when d becomes too large, the number of polynomials increases dramatically. To avoid this problem, polynomials with less importance are detected and eliminated in order to reduce the computation time considerably.

$$u(\xi) \approx \sum_{i=0}^{P} y_i \psi_i(\xi) \tag{4.15}$$

Where ξ are independent random parameter vectors and the coefficients y_i are obtained by least-square optimisation. Once the surrogate model has been completed it is necessary to check it against the real model. For this purpose the Leave-One-Out error is calculated by comparing the results of the surrogate model with those of the real model for a number of generations. An error that is too large indicates that the surrogate model does not fit correctly and is therefore not representative. Another advantage of the PCE is the ease of calculating the sensitivity of each uncertainty through the sobols indices. These indicate the relative impact of each parameter on the overall variance of the objective of interest. Thus, parameters with low Sobol indices can be changed to deterministic parameters and thus reduce the calculation costs. The limit below which they are considered non-influential is set as :

$$Threshold = \frac{1}{\#stoch\,parameters} \tag{4.16}$$

4.4.2 Stochastic space

The stochastic space captures the uncertainty of certain parameters of the system. It is determined by a Gaussian or Uniform distribution for which the value of the standard deviation must be specified. In the context of this thesis, the main uncertainty concerns the wind speed. According to the stochastic method used, the ϵ_i coefficients follow a Gaussian distribution centred in zero and of unit deviation. In this way a power profile is randomly generated at each simulation and the impact of this stochasticity is then quantified through the sobols indices. The number of coefficients used is ten in order to obtain a sufficiently realistic profile in the simulations. Apart from this wind-related uncertainty, there are others concerning the system itself. Indeed, the minimum and maximum current density fixed within the cell of the electrolyser is adapted by means of converters. The latter are not ideal and have a certain error with respect to the current required through the electrolysers. It is therefore important to include this uncertainty in the model in order to know the consequences. The table 4.1 summarises the uncertainties and their distributions taken into account.

	Distribution	**Deviation**	**Source**
Uncertainty parameters of the wind speed (x10) ϵ_i	Gaussian	$1[-]$	
Minimum current density J_{min}	Uniform	$\pm 2\%$	[45]
Maximal current density J_{max}	Uniform	$\pm 2\%$	[45]

Table 4.1: Stochastic space of the uncertainty quantification

In summary, when quantifying uncertainty, the uncertainty of the parameters is propagated according to their well-defined distribution and the analysis of the sobols indices allows to know the impact of each of them on the standard deviation of the studied objective in question. The already high number of coefficients for the stochastic process limits the addition of other sources of uncertainty for computational cost reasons.

Chapter 5

Results and discussion

This chapter presents the results obtained from the optimization of the objectives presented above. This allows us to determine an optimal design based on the objectives. A sensitivity study is then carried out through the parameters of the model presenting a stochasticity.

5.1 Deterministic design optimisation

The first phase corresponds to the optimisation of the objectives presented in the previous sections. Only the design variables can be modified here by the NSGA algorithm. The stochastic parameters remain deterministic at this stage. The power profile generated by the stochastic process is thus the same for all the optimisation simulations.

5.1.1 Wide-ranging variables

The first phase of the optimisation is carried out on a very large design space in terms of variables. The aim is to identify interesting areas for a second, more targeted optimisation. The table 5.1 shows the principal values used for the parameters and variables of the optimisation.

For this first optimisation, 40 generations of 30 individuals are generated one by one by the NSGA-II algorithm. This is a three-dimensional optimisation minimising the three objectives presented in the previous chapter.

$$Obj_1 = min(\frac{\sum P_{grid} + E_{loss}}{\sum P_{WF} + \sum P_{grid}}) \tag{5.1}$$

$$Obj_2 = min(LF_{PEM}) \tag{5.2}$$

$$Obj_3 = min(LF_{bat}) \tag{5.3}$$

A first interesting result is the evolution of the lifetime of electrolysers and batteries as a function of the proportion of energy from the grid and lost (Figure 5.1). There is a strong correlation between these different objectives. To increase the lifetime of electrolysers, it is necessary to accept an increase in the amount of energy "wasted" by the system. As for the life of the batteries, initially high, it drops rapidly before increasing again just as quickly. This excessively high lifetime at certain times is explained by the fact that the batteries are almost inactive. Indeed, their degradation is quantified on the basis of the number of complete cycles performed, hence the very high lifetimes when the batteries are not used much or at all. For a very small part of the energy lost, almost all the wind energy is directly taken over by the electrolyser. This means that the electrolyser is constantly in a dynamic state, which results

in considerable damage. Fortunately, below 10 % of energy losses, the degradation of the electrolyser rapidly decreases to acceptable values, knowing that the life of an electrolyser is generally estimated between 60,000 and 100,000 hours (about 6 and 10 years of continuous operation). Otherwise, the rapid decrease in battery life. These compensate for the reduced use of electrolysers with low current densities. Beyond 10 % dependence on the grid, the life span of the components increases seriously. However, the share of the grid becomes far too high to consider the system interesting. This shows a very poor flexibility in relation to the wind farm's electricity production, as external help is constantly needed to avoid having to switch off the electrolyser at low current densities. In order to better understand the phenomena described above, it is interesting to analyse the link between the optimisation objectives and the variables.

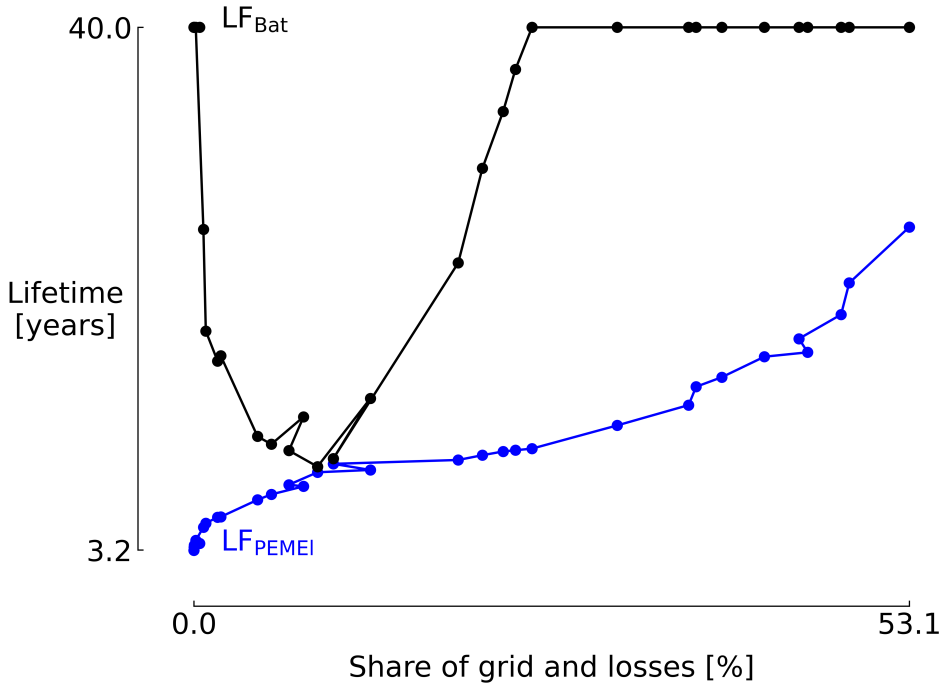

Figure 5.1: NSGA-II Optimization. Evolution of the PEM EL (blue) and battery (orange) lifetimes according to the share of grid and losses

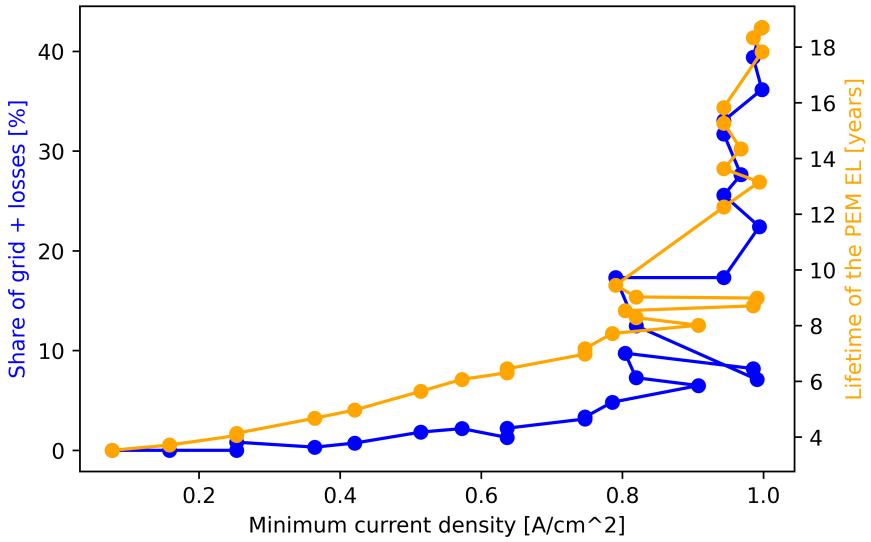

Figure 5.2: NSGA-II Optimization. Evolution of the PEM EL lifetime and the share of grid and losses according to the minimum current density in the cell.

Figure 5.2 shows the evolution of the electrolyser's lifetime and the share of grid and losses in relation to the minimum current density allowed in the cell. The result obtained is quite logical, when this minimum density increases, the electrolyser is less often in dynamic regime which allows to decrease its degradation. In this case, below $0.3[A/cm^2]$, the lifetime of the electrolyser is considered far too short (<5 years) to be integrated into a desired flexible system. Therefore, a new design space does not allow the minimum current density to fall under this value. The other obvious observation in Figure 5.2, is the strong correlation between the increase in the lifetime of the electrolysers and the share of grid and losses. A decrease in electrolyser degradations is undeniably the cause of a loss of system flexibility. Indeed, reducing the operating range of the electrolyser increases the chances of having to feed it from the grid because of empty batteries. By the way, the degradation of the batteries is mainly influenced by the virtual maximum current density as shown in figure 5.3. The latter never exceeds $4[A/cm^2]$, beyond which the degradation of the battery is far too great without improving the other objectives. However, the observed lifetimes remain most of the time quite acceptable compared to what can be expected from a lithium-ion battery (5 to 20 years depending on use).

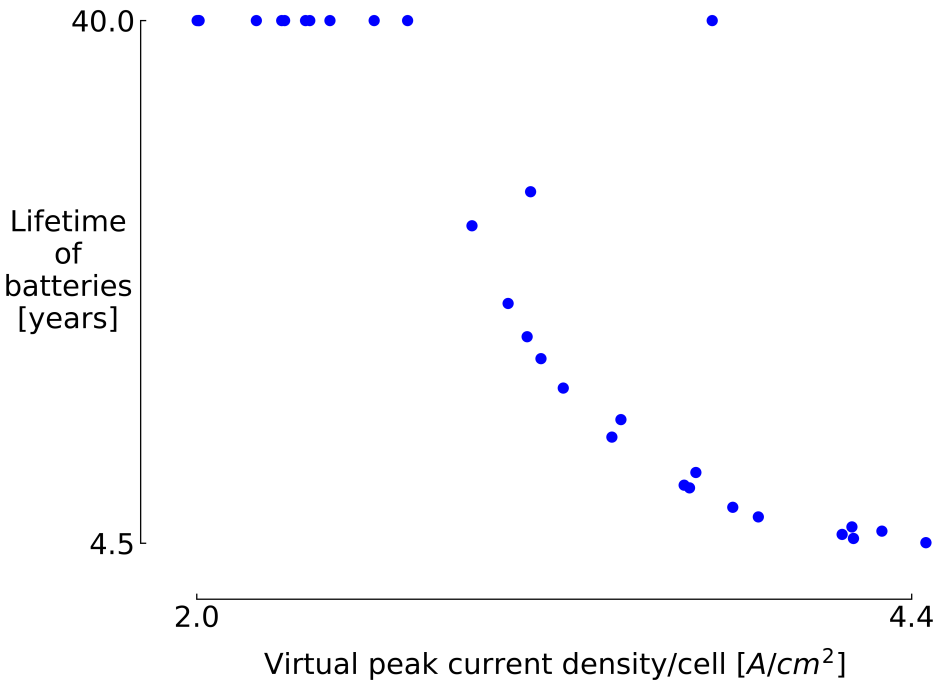

Figure 5.3: NSGA-II Optimization. Evolution of the PEM EL lifetime and the share of grid and losses according to the minimum current density in the cell.

Finally, it is also interesting to analyse the evolution of the lifetime of the electrolysers and the share of the grid and losses in relation to the maximum virtual current density. Figure 6.22 shows again a strong correlation between these two objectives with respect to this variable. It can be observed that below $2.75[A/cm^2]$, either the lifetime of the electrolysers is less than 5 years, or the share of the grid and losses is greater than 20%. It is obvious that beyond these values the system is no longer relevant and therefore the design space is redefined.

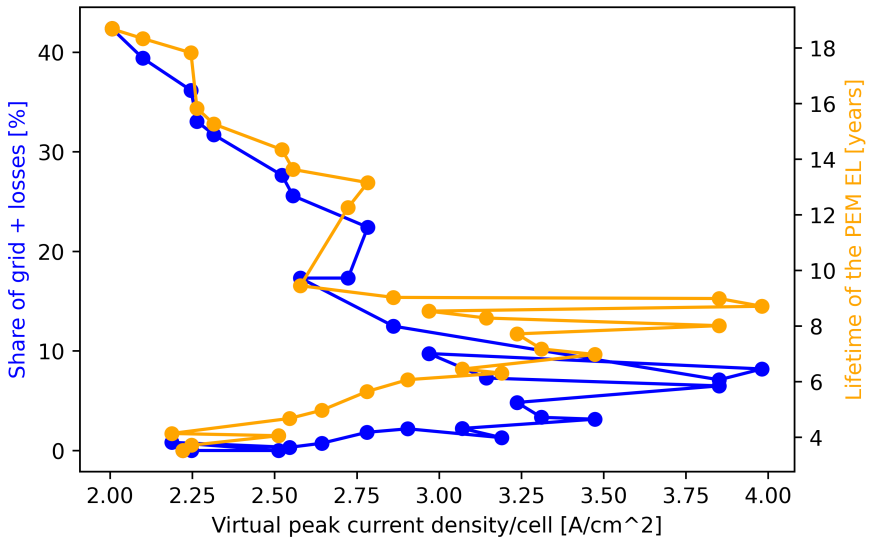

Figure 5.4: NSGA-II Optimization. Evolution of the PEM EL lifetime and the share of grid and losses according to the minimum current density in the cell.

	Values	Units	Source
Minimal current density J_{min}	0-1	$[A/cm^2]$	
Virtual peak current density J_{peak}	2-5	$[A/cm^2]$	
Maximal current density J_{max}	2	$[A/cm^2]$	
Thermal capacitance of the stack C_{th}	42 045	$[J/K]$	[45]
Thermal resistance of the stack R_{th}	0.0817 K/W	$[K/W]$	[45]
Ambiant temperature T_{amb}	10	$[°C]$	[54]
Cell active area A	50	$[cm^2]$	[44]
Membrane thickness δ_M	178	$[\mu m]$	[44]
Hydrogen partial pressure p_{H_2}	15	$[bar]$	[44]
Oxygen partial pressure p_{0_2}	1	$[bar]$	[44]
Activation energy at the anode E_a	76 000	$[J/mol]$	[55]
Activation energy at the cathode E_c	4300	$[J/mol]$	[55]
Anode exchange current density at T_{ref} $i_{0a,ref}$	10^{-9}	$[A/cm^2]$	[44]
Cathode exchange current density at T_{ref} $i_{0c,ref}$	10^{-3}	$[A/cm^2]$	[44]
Charge transfer coefficient at the anode α_a	0.5	$[-]$	[44]
Charge transfer coefficient at the cathode α_c	2	$[-]$	[44]

Table 5.1: Values of the principal variables and parameters of the model

Impact of batteries

So far, no comparative results have yet been obtained between the design with and without batteries. Now that two designs have been determined, it is interesting to compare these results with a system without batteries. The first finding is the obvious change in proton exchange membrane degradation (Figure 5.5). These are up to twice as high in the system without battery compared to the other two designs. This can be explained by the fact that the model without the battery is constantly in dynamic regime.

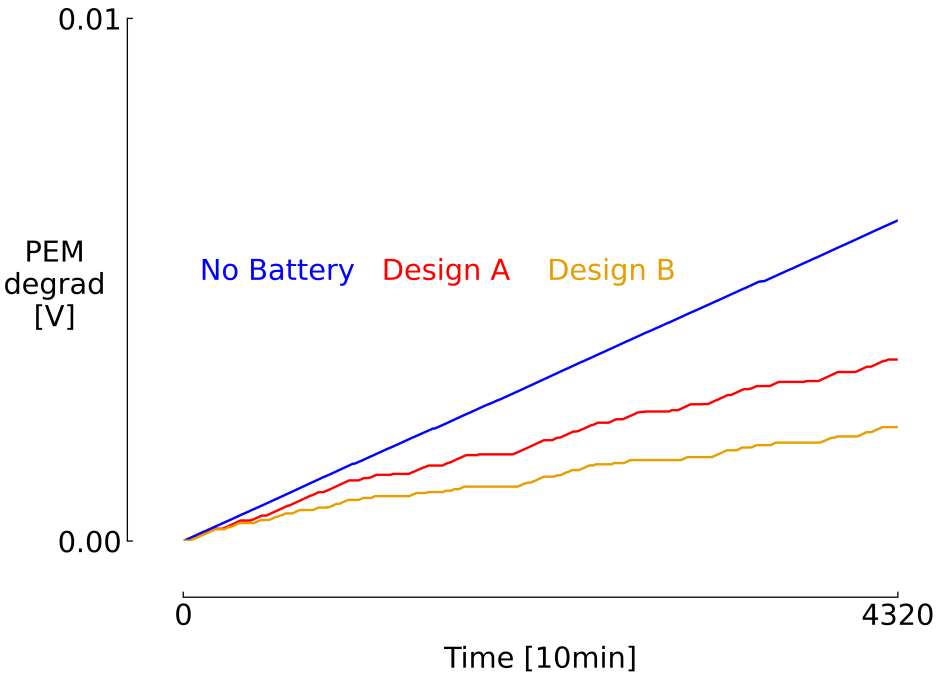

Figure 5.5: Evolution of the PEM degradation according to both design and a system whitout batteries.

The second interesting result is the evolution of the hydrogen productions only due to the power supplied by the wind farm 5.6). The share of hydrogen produced by the grid has therefore been subtracted in the case of design A and B. At first sight, the productions seem very similar. The system without batteries produced a mass of hydrogen equivalent to 877.29 MWh, while design A produced 884.49 MWh. This represents an increase in production of about 1%. This increase is due to the limitation of the maximum current density that can be applied with the batteries. Design A is therefore more efficient in terms of hydrogen production than the system without batteries. Design B produced the equivalent of 870.14 MWh. This decrease in performance is due to losses when the batteries are full.

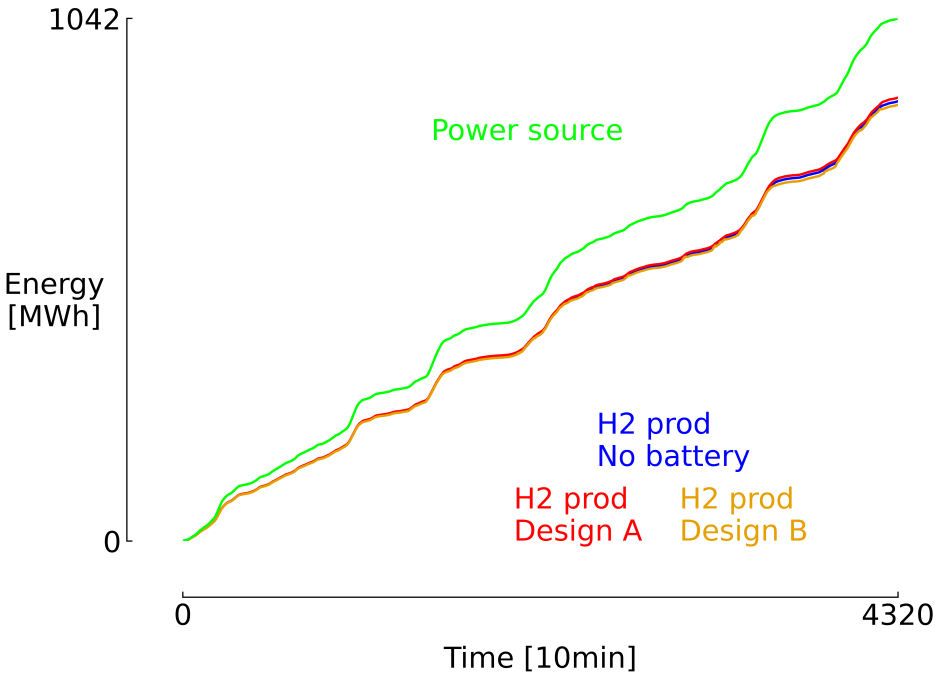

Figure 5.6: Evolution of the equivalent hydrogen energy production according to both design and a system whitout batteries. The green curve represent the cumulative energy supplied by the wind farm.

5.2 Targeted ranges of variables

Following the observations made in the previous section, a new design space has been defined (Table 5.2). This is reduced and allows us to focus on the areas of optimisation that are interesting for the system.

	Values	Units
Minimal current density J_{min}	0.3-1	$[A/cm^2]$
Virtual peak current density J_{peak}	2.75-4	$[A/cm^2]$

Table 5.2: New design space

For this new optimisation, 50 generations of 40 individuals are generated one by one by the NSGA-II algorithm. The evolution of the three objectives is illustrated in Figure 5.7. The share of network and losses is here limited to 25 % which allows to explore a larger number of interesting design points than in the previous optimisation.

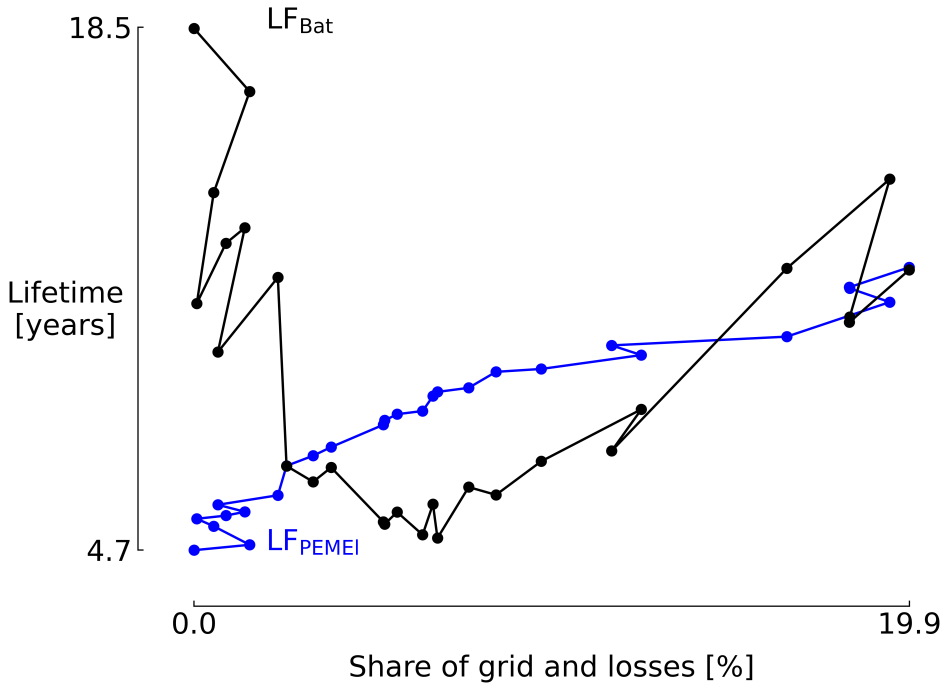

Figure 5.7: NSGA-II Optimization. Evolution of the PEM EL and battery lifetime according to the share of grid and losses.

At first sight, it seems that the optimisation is not finished. However, it should be remembered that the optimisation is carried out in three dimensions and a visually ideal pareto front is not expected as in 2D optimisation. A check was carried out to ensure that each of the individuals in the final generation is non-dominant compared to the rest of the population. The test proved successful as each individual has at least one objective that is better optimised than any other individual. Having done so, we can still observe the

same behaviour of the objectives as in the previous section. The reason for this is of the same nature as the explanations already given. In fact, this more precise optimisation allows to determine interesting design points in order to study their robustness under stochastic behaviour. A share of grid and losses of maximum 10 % is considered as the acceptable limit for the system and a minimum lifetime of 6 years for the electrolyser. Two interesting design points that meet these limits are chosen as shown in figure 5.8.

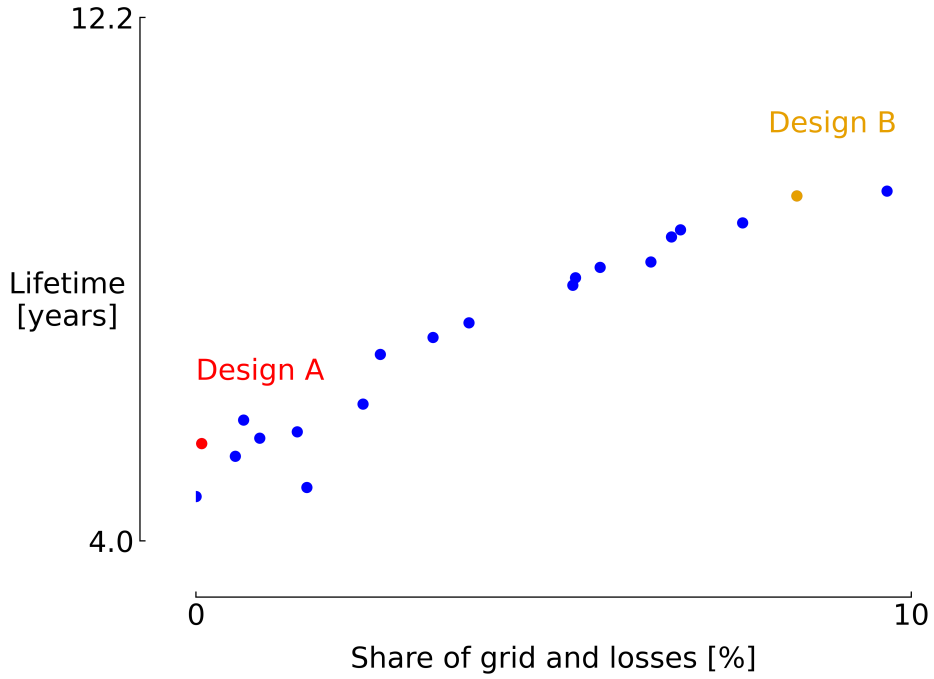

Figure 5.8: NSGA-II Optimization. Design points selected to undergo uncertainty quantification.

Design A tends to minimise the share of grid and losses while keeping the lifetime of the electrolyser acceptable. Design B, on the other hand, tends to maximise the lifetime of the electrolyser while limiting the share of grid and losses to a more or less acceptable value. The values of the variables and objectives for these two designs are presented in table 5.3.

	Design A	**Design B**	**Units**
Minimal current density J_{min}	0.579	0.945	$[A/cm^2]$
Virtual peak current density J_{peak}	3.06	3.40	$[A/cm^2]$
Share of grid and losses Obj_1	0.667	8.40	$[\%]$
Lifetime of the electrolyser Obj_2	5.89	9.40	$[years]$
Lifetime of the battery Obj_3	9.92	6.15	$[years]$

Table 5.3: Design variables and objective values of design A and B

5.3 Uncertainty quantification

Up to now, optimisation has been based on a deterministic power profile. However, it is obvious that there is a random uncertainty in the wind speed at the wind turbines. Therefore, uncertainties will be propagated through the stochastic process via the uncertainty coefficients ϵ_i in order to study their impact on the presented objectives. The stochastic procedure requires a high degree of polynomial in order to obtain an acceptable Leave-One-Out-Error (LOOE). Therefore a polynomial of order 3 is used with a total of 12 uncertainties.

5.3.1 Objective 1 : share of grid and losses

The first objective whose uncertainty is studied is the share of the grid used and the losses due to full batteries at high power. The first information observed is the LOOE representing the error between the surrogate model and the real model. The errors encountered are particularly high (10-20%) despite the use of a third order polynomial. Indeed, the uncertainties propagated by the ϵ_i coefficients are important and it is difficult for the PCE to capture their exact behaviour. The use of a fourth-order polynomial makes the situation worse and therefore the third order is used. The table 5.4 shows the LOOE for each of the two designs. Another reason for these high errors could be the impossibility of the objective in question being negative. Indeed, the values obtained are sometimes close to zero or even zero but cannot be negative. The surrogate model, on the other hand, assumes the possibility of obtaining a negative result, which results in significant errors when calculating the LOOE. Design A logically has a lower average lifetime than design B. Indeed, the latter with its higher minimum current density reduces the operating time of the electrolyser under dynamic conditions.

Design	Mean	Standard deviation	LOOE
A	$5.36[\%]$	$4.71[\%]$	$12.38[\%]$
B	$8.62[\%]$	$6.93[\%]$	$15.11[\%]$

Table 5.4: PCE results for the share of grid and losses.

Although the errors are high, the probability density functions are nevertheless representative of the behaviour of the system. The averages obtained in the table confirm the greater autonomy of Design A. Moreover, the latter also has a lower standard deviation, thus reducing the uncertainty on the use of the network by the system and its losses. The figure 5.10 is a graphical representation of these results.

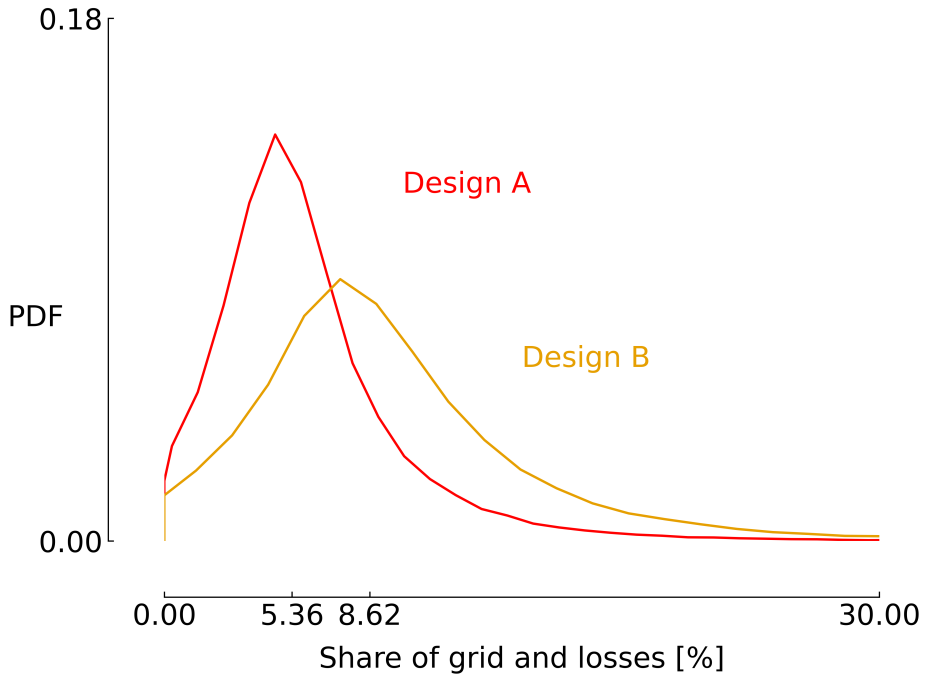

Figure 5.9: Probability density function of the share of grid and losses according to both Design A and B.

The main obesrvation made on the basis of the results obtained remains the important uncertainty inflicted by the epsilon coefficients. These inflict a large standard deviation even for the most robust design. The minimum current densities J_{min} and J_{max} have none influence on the system compared to the epsilon coefficients. The uncertainty on the grid usage is rather constraining as it is not always suitable. Nevertheless, one solution would be to use the system intelligently with respect to the state of the grid. Relieving the grid when it is overloaded by topping up the batteries could make the use of the grid much less problematic than it seems. In summary, design A is not only the most autonomous but also the least uncertain. However, this uncertainty is still considerable and could make the system unpredictable. Therefore, it would be interesting to optimise the use of the grid when it is overloaded through a techno-economic study. The most robust solution is finally offered by Design A and it allows at the same time to maximise the autonomy and flexibility of the system. Indeed, the more this objective is minimised, the more the system is able to convert a maximum of the energy supplied without the need for external support (grid) and without the need to reduce the power generated by the wind farm (losses).

Figure 5.10: Sobol's indices

5.3.2 Objective 2 : lifetime of the electrolyser

The second objective studied is the life span of the electrolysers extrapolated to the period studied. Indeed, as a reminder, this lifetime is calculated on the basis of a permanent degradation caused by the dynamic regimes. This is then converted into a lifetime in relation

to a maximum drop in efficiency. The Leave-One-Out-Error obtained is again significantly high (Table 5.5). The reasons are the same as for the previous objective. The ϵ_i coefficients inflict such uncertainty that it is complex for the PCE to capture the exact behaviour. Moreover, the degradations, sometimes very close to zero, once again make the surrogate model find negative values, which is obviously impossible.

Design	Mean	LOOE
A	$6.16[years]$	$11.64[\%]$
B	$8.97[years]$	$10.09[\%]$

Table 5.5: PCE results for the lifetime of the electrolysers.

The table 5.5 does not show the standard deviation for the following reason. The conversion of degradation to lifetime is not a directly proportional relationship but rather inversely proportional. As a result, the probability function is no longer a Gaussian but more likely follows a logarithmic style distribution (Figure 5.11). However, the averages obtained are very significant and clearly demonstrate that design B offers a longer durability of the system at the electrolyser level. Furthermore, this distribution clearly shows that it is unlikely to achieve very low lifetimes. This has the advantage that the minimum expected lifetime can be easily estimated. Design A therefore shows, as expected, a higher degradation of its electrolysers without leading to too low lifetimes. Therefore, in view of the results obtained for the previous objective, the Design A remains the most optimised and robust solution in the spirit of an autonomous and flexible system.

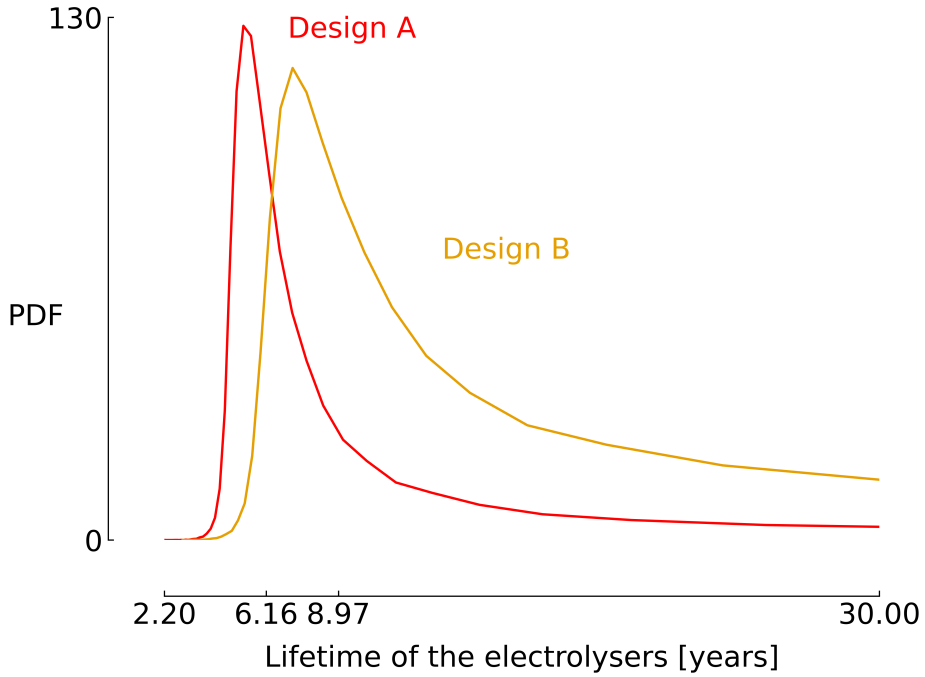

Figure 5.11: Probability density function of the lifetime of the electrolysers according to both Design A and B.

In terms of the Sobol indices, it is again very clear that the uncertainty is mainly influenced by the ϵ_i coefficients of the stochastic process. These are responsible for more than 90% of the variance of the electrolyser degradations. While the minimum and maximum current densities are insignificant compared to the system behaviour.

5.3.3 Objective 3 : Battery lifetime

This last objective aims to minimise the number of complete charge cycles performed by the batteries in order to maximise their life span. The main data collected by the algorithm at the end of each simulation is therefore the number of cycles. The LOOE is again important for the reasons already explained above. The table 5.6 gives the characteristics of the probability functions of the two designs. Design A has a lower number of cycles than Design B. This result is not surprising, as the range of operation of the electrolyser is lower in this design and the batteries are used less often by the system. The first design therefore offers a longer battery life for the system. In addition, the standard deviation obtained for this first design is smaller than that of Design B. In this way it can be stated that Design A is both more robust and better optimised than Design B.

Design	Mean	Standard deviation	LOOE
A	$4.48[-]$	$3.24[-]$	$11.72[\%]$
B	$6.52[-]$	$4.55[-]$	$13.89[\%]$

Table 5.6: PCE results for the number of cycles.

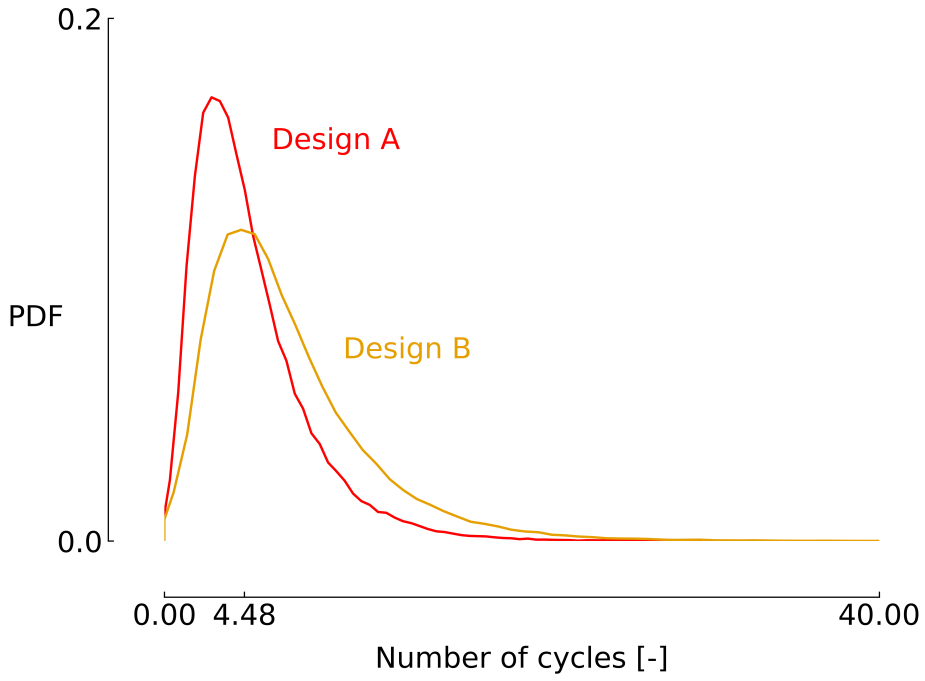

Figure 5.12: Probability density function of the complete cycles of the batteries according to both Design A and B.

5.3.4 Efficiency of the cells

The internal efficiency of the electrolyser is not listed as a target, but it is still interesting to know the uncertainty about it. This determines the efficiency with which the energy entering the electrolyser is converted into hydrogen. This efficiency is a function of the current density through the electrolyser, the temperature within the electrolyser and also the degradation. The LOOE is still quite high but is still lower than for previous targets (Table 5.7). This can be explained by the fact that, unlike the others, the yield never reaches a value close to zero. The surrogate model therefore always generates probable values. Nevertheless, the uncertainty propagated by the coefficients of the stochastic process is not fully captured by the PCE.

Design	Mean	Standard deviation	LOOE
A	$80.36[\%]$	$4.96[\%]$	$6.45[\%]$
B	$78.75[\%]$	$6.70[\%]$	$7.27[\%]$

Table 5.7: PCE results for the cell efficiency

The table 5.7 shows that the average efficiency of Design A is slightly higher than Design B. This observation is logical because at low current density the electrical overpotentials are less important than at high density and therefore the efficiency is better. The standard deviation displayed by Design A is also higher and therefore indicates a better robustness than its neighbouring Design. Figure 5.13 confirms these findings.

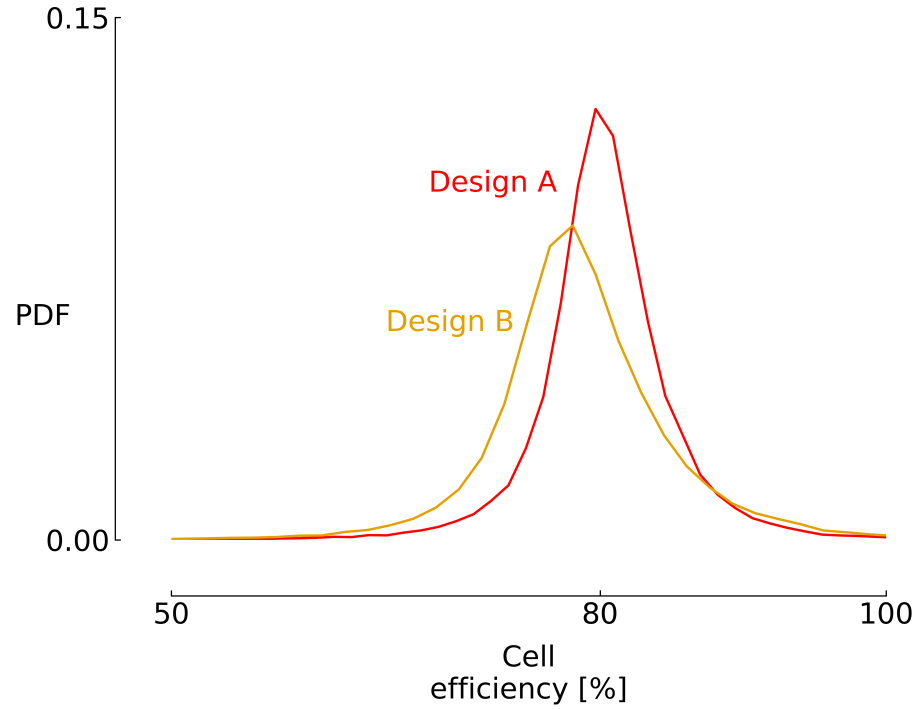

Figure 5.13: Probability density function of the electrolyser cell efficiency according to both Design A and B.

Chapter 6

Conclusion

In the context of the climate crisis, the transition from fossil fuels to renewable sources is more urgent than ever. The intermittency of these energies forces innovative solutions to be found to shift the energy produced in time. Among these solutions is hydrogen. Its abundant presence in water and its zero-carbon potential make it a prime candidate. The use of hydrogen would allow the storage of surplus electricity production through the so-called Power-to-Hydrogen. This chemical energy can then be fed back into the grid as electricity or used in its original form as a zero-emission fuel.

Nevertheless, there are various technologies for converting electricity into hydrogen through the electrolysis of water. Not all of these technologies are suitable for the volatility of renewable sources. After a review of the literature, it appeared that proton exchange membrane electrolysis (PEM) is currently the most appropriate technology to be coupled with a renewable source. Indeed, alkaline water electrolysis (AWE) has a reaction time that is far too long (10 minutes) to ensure a minimum of flexibility. And this despite its maturity of development. Solid oxide electrolysis (SOEC) is promising but remains at the research stage.

This thesis proposes the development of a PEM electrolyzer model with dynamic thermal behaviour. Indeed, the influence of temperature on cell performance has been shown to be too important to neglect its temporal evolution. This model is then connected to a wind farm simulated by a stochastic process. In view of the low efficiency of the electrolyser at high load and the significant degradation caused by a dynamic regime, it was decided to integrate batteries into the system. The aim of these batteries is to store energy beyond a certain operating range and to transmit it when the power generated by the wind farm is too low. Finally, the grid is used when the energy contained in the batteries is too low.

Once the model was completed and validated, a deterministic optimisation was performed with the Nondominated Sorting Genetic Algorithm (NSGA-II) for which the main design variables were the number of cells and the minimum current density allowed in the cell of the electrolyser. It appears that to minimise the degradation inflicted on the electrolyser, the system must reduce its autonomy and flexibility. Indeed, for an electrolyser lifetime of 9 years, the share of the grid and losses reaches 9%. However, if a lower lifetime is allowed (6 years), the share of grid and losses drops considerably below one percent. Logically, it is found that the life of the batteries is inversely proportional to the life of the electrolysers. As a result of these observations, two designs were defined. The first one improves the autonomy and flexibility of the system (0.67%) by reducing the lifetime of the electrolysers

(5.8 years). The second design predicts the lifetime of the electrolysers (9.4 years) at the expense of its autonomy and flexibility (8.4%).

Finally, the sensitivity of the system across the objectives was evaluated by Polynomial Chaos Expansion (PCE). The uncertainty propagated is characteristic of the wind speeds at the wind turbines. Although significant errors were found between the real model and the overrogate model ($\approx 10\%$), it was still possible to draw conclusions. The first design confirms the trend of better flexibility and autonomy for many different scenarios. In addition, it is more robust than the design that favours the lifetime of the electrolysers.

In conclusion, the design of a Power-to-Hydrogen system coupled with batteries allows to extend the lifetime of the system while preserving a minimum of autonomy and flexibility. However, a more in-depth study of the proton exchange membrane degradation phenomena is required to provide more precision in the calculation of its lifetime.

Bibliography

[1] IRENA (2018), Hydrogen from renewable power: Technology outlook for the energy transition, International Renewable Energy Agency, Abu Dhabi.

[2] https://www.connaissancedesenergies.org/bp-statistical-review-world-energy-2022-les-chiffres-cles-de-lenergie-dans-le-monde-220629

[3] IRENA (2019), Innovation landscape brief: Renewable Power-to-Hydrogen, International Renewable Energy Agency, Abu Dhabi.

[4] Tan Wang, Yu Gong, Chuanwen Jiang (2014) *A review on promoting share of renewable energy by green-trading mechanisms in power system* ,Vol.40, Renewable and Sustainable Energy Reviews. p. 923-929.

[5] G. Pan, W. Gu, Y. Lu, H. Qiu, S. Lu and S. Yao, "Optimal Planning for Electricity-Hydrogen Integrated Energy System Considering Power to Hydrogen and Heat and Seasonal Storage," in IEEE Transactions on Sustainable Energy, vol. 11, no. 4, pp. 2662-2676, Oct. 2020, doi: 10.1109/TSTE.2020.2970078.

[6] IRENA (2019), Hydrogen: A renewable energy perspective, International Renewable Energy Agency, Abu Dhabi

[7] Gilles Notton, Marie-Laure Nivet, Cyril Voyant, et al. (2018) *Intermittent and stochastic character of renewable energy sources: Consequences, cost of intermittence and benefit of forecasting* ,Vol.40, Renewable and Sustainable Energy Reviews. p. 96-105.

[8] European Comission (2020) *How hydrogen is lighting the way for more sustainable energy systems, biodegradable food packaging that increases shelf life and new techniques in ceramic manufacturing*, Vol.94, Research*eu magazine.

[9] Gerda Gahleitner (2013) *Hydrogen from renewable electricity: An international review of power-to-gas pilot plants for stationary applications*, Vol.38, International Journal of Hydrogen Energy. p. 2039-2061.

[10] Schlögl, Robert. Chemical Energy Storage, Berlin, Boston: De Gruyter, 2022. https://doi.org/10.1515/9783110608458

[11] Fritz R. Kalhammer, Thomas R. Schneider (1976) *ENERGY STORAGE*, Annu. Rev. Energy. 1976.1:311-343

[12] Oesper, Ralph; Speter, Max (1937). "The Faraday-Whewell correspondence concerning electro-chemical terms". The Scientific Monthly. 45 (6): 535–546

[13] Emmanuel Zoulias, Elli Varkaraki, Nicolaos Lymberopoulos, et al. *A review on water electrolysis*.

[14] Ali Keçebaş, Muhammet Kayfeci, Mutlucan Bayat (2019),*Chapter 9 - Electrochemical hydrogen generation*,Solar Hydrogen Production,Academic Press, p. 299-317.

[15] Martín David, Carlos Ocampo-Martínez, Ricardo Sánchez-Peña (2019), *Advances in alkaline water electrolyzers: A review*, Vol. 23, Journal of Energy Storage, p. 392-403

[16] A. Manabe, M. Kashiwase, T. Hashimoto, T. Hayashida, A. Kato, K. Hirao, I. Shimomura, I. Nagashima (2013), *Basic study of alkaline water electrolysis*, Vol. 100,Electrochimica Acta, p. 249-256.

[17] Jörn Brauns and Thomas Turek (2020) *Alkaline Water Electrolysis Powered by Renewable Energy: A Review*, Journal of Cleaner Production.

[18] Md Mamoon Rashid, Mohammed K. Al Mesfer, Hamid Naseem, Mohd Danish (2015), *Alkaline Water Electrolysis Powered by Renewable Energy: A Review*,Vol.4, International Journal of Engineering and Advanced Technology (IJEAT), p. 80-93

[19] M. Schalenbach, A. R. Zeradjanin, O. Kasian, S. Cherevko, and K. J. J. Mayrhofer (2018), *A perspective on low-temperature water electrolysis - Challenges in alkaline and acidic technology*, Vol. 13,Int. J. Electrochem. Sci., p. 1173–1226.

[20] Julian Parra-Restrepo. Caractérisation des hétérogénéités de fonctionnement et dedégradation au sein d'un électrolyseur à membrane échangeuse de protons(PEM) .Sciences de l'ingénieur[physics]. Université de Lorraine,2020

[21] M. Carmo, D. L. Fritz, J. Mergel, and D. Stolten (2013), *A comprehensive review on PEM water electrolysis*, Vol. 38, Int. J. Hydrogen Energy, p. 4901–4934.

[22] Frano Barbir (2005),*PEM electrolysis for production of hydrogen from renewable energy sources*,Vol. 78 Solar Energy, p. 661-669.

[23] Hiroshi Ito, Tetsuhiko Maeda, Akihiro Nakano, Hiroyasu Takenaka (2011), *Properties of Nafion membranes under PEM water electrolysis conditions*, Vol. 36, International Journal of Hydrogen Energy, P. 10527-10540.

[24] S. Siracusano, N. Van Dijk, R. Backhouse, L. Merlo, V. Baglio, A.S. Aricò (2018), *Degradation issues of PEM electrolysis MEAs*, Vol.123, Renewable Energy, p. 52-57

[25] Jan van der Merwe, Kenny Uren, George van Schoor, Dmitri Bessarabov (2014), *Characterisation tools development for PEM electrolysers*, Vol.39, International Journal of Hydrogen Energy, p. 14212-14221.

[26] CONVION Fuel Cell Systems, `https://convion.fi/technology/`

[27] Arunkumar Pandiyan, MTech, PhD Aarthi Uthayakumar, MTech Rengaraj. *Review of solid oxide electrolysis cells: a clean energy strategy for hydrogen generation*, Vol.8, Nanomaterials and Energy. p. 2-22.

[28] Meng Ni, Michael K.H. Leung, Dennis Y.C. Leung (2008), *Technological development of hydrogen production by solid oxide electrolyzer cell (SOEC)*, Vol. 33, International Journal of Hydrogen Energy, p. 2337-2354,

[29] Fu Wang, Lei Wang, Houcheng Zhang, Lan Xia, He Miao, Jinliang Yuan (2021), *Design and optimization of hydrogen production by solid oxide electrolyzer with marine engine waste heat recovery and ORC cycle*, Vol.229, Energy Conversion and Management.

[30] Alexander Buttler, Hartmut Spliethoff (2018), *Current status of water electrolysis for energy storage, grid balancing and sector coupling via power-to-gas and power-to-liquids: A review*, Vol. 82, Renewable and Sustainable Energy Reviews, p. 2440-2454.

[31] Angeliki Loukatoua, Sydney Howell, Paul Johnson, Peter Duck (2018) *Stochastic wind speed modelling for estimation of expected wind power output*, Vol.228, Applied Energy. p. 1328-1340.

[32] J. Jonkman, S. Butterfield, W. Musial, and G. Scott (2017) *Definition of a 5-MW Reference Wind Turbine for Offshore System Development*, National Renewable Energy Laboratory.

[33] O. Schmidt, A. Gambhir, I. Staffell, A. Hawkes, J. Nelson, S. Few (2017) *Future cost and performance of water electrolysis: An expert elicitation study*, Vol.42, International journal of hydrogen energy. p. 30470-30492.

[34] Yujing Guo et al 2019 IOP Conf. Ser.: Earth Environ. Sci. 371 042022

[35] Somayeh Toghyani, Soheil Fakhradini, Ebrahim Afshari, Ehsan Baniasadi, Mohammad Yaghoub Abdollahzadeh Jamalabadi, Mostafa Safdari Shadloo (2019) *Optimization of operating parameters of a polymer exchange membrane electrolyzer*, Vol.44, International Journal of Hydrogen Energy. p. 6403-6414.

[36] Eng. Waseem Saeeda, Eng. Ghaith WarkozekDr (2015) *Modeling and Analysis of Renewable PEM Fuel Cell System*, Vol.74, Energy Procedia. p. 87 – 101.

[37] D.S. Falcao, A.M.F.R. Pinto (2020) *A review on PEM electrolyzer modelling: Guidelines for beginners*, Journal of Cleaner Production.

[38] Haluk Görgün (2006) *Dynamic modelling of a proton exchange membrane (PEM) electrolyzer*, Vol.31, International Journal of Hydrogen Energy. p. 29 – 38.

[39] M. Maier, K. Smith, J. Dodwell, G. Hinds, P.R. Shearing, D.J.L. Brett (2022), *Mass transport in PEM water electrolysers: A review*, Vol.47, International Journal of Hydrogen Energy, p. 30-56.

[40] Pyoungho Choia, Dmitri G. Bessarabovb, Ravindra Dattaa, (2004) *A simple model for solid polymer electrolyte (SPE) water electrolysis*, Vol.15, Solid State Ionics. p. 535 – 539.

[41] Ángel Hernández-Gómez, Victor Ramirez, Damien Guilbert (2020) *Investigation of PEM electrolyzer modeling: Electrical domain, efficiency, and specific energy consumption*, Vol.45, International Journal of Hydrogen Energy, p. 14625-14639.

[42] K. P. Adzakpa, Kodjo Agbossou, Yves Dubé, Michel Dostie, Michael Fournier and Alain Poulin (2008), *PEM fuel cells modeling and analysis through current and voltage transient behaviors.* Vol.3, IEEE Transactions on Energy Conversion, p. 581-591.

[43] Yodwong, B.; Guilbert, D.; Hinaje, M.; Phattanasak, M.; Kaewmanee, W.; Vitale, G. (2021), *Proton Exchange Membrane Electrolyzer Emulator for Power Electronics Testing Applications.* Processes, 9, 498.

[44] Tijani AS, et al., Investigation of the effect of charge transfer coefficient (CTC) on the operating voltage of polymer electrolyte membrane (PEM) electrolyzer, International Journal of Hydrogen Energy (2018), https://doi.org/10.1016/ j.ijhydene.2018.03.111

[45] R. García-Valverde, N. Espinosa, A. Urbina (2012), *Simple PEM water electrolyser model and experimental validation*, Vol.37, International Journal of Hydrogen Energy, p. 1927-1938.

[46] Scheepers, Fabian and Stähler, Markus and Stähler, Andrea and Rauls, et al. (2020), *Improving the Efficiency of PEM Electrolyzers through Membrane-Specific Pressure Optimization*, Vol.13, Energies, p. 4901-4933

[47] ACS Cent. Sci. 2017, 3, 10, 1063–1069 Publication Date:September 7, 2017

[48] Angeliki Loukatou, Sydney Howell, Paul Johnson, Peter Duck (2018), *Optimal joint strategy of wind battery storage unit for smoothing and trading of wind power*, Vol.151, Energy Procedia, p. 91-99.

[49] K. Deb, A. Pratap, S. Agarwal and T. Meyarivan, "A fast and elitist multiobjective genetic algorithm: NSGA-II," in IEEE Transactions on Evolutionary Computation, vol. 6, no. 2, pp. 182-197, April 2002

[50] Stefania Siracusano, Stefano Trocino, Nicola Briguglio, Fabiola Panto, Antonino S. Arico, (2020) *Analysis of performance degradation during steady-state and load-thermal cycles of proton exchange membrane water electrolysis cells*, Vol.468, Journal of Power Sources.

[51] Georgios Papakonstantinou, Gerardo Algara-Siller, Detre Teschner, Tanja Vidakovic-Koch, Robert Schlogl, Kai Sundmacher, (2020) *Degradation study of a proton exchange membrane water electrolyzer under dynamic operation conditions*, Vol.280, Applied Energy.

[52] *Multi-objective Optimisation in Python, Pymoo*,`https://pymoo.org/algorithms/moo/nsga2.html`

[53] Bruno Sudret (2008) *Global sensitivity analysis using polynomial chaos expansions*, Vol.93, Reliability Engineering System Safety, p. 964-979.

[54] WEATHER AND CLIMATE, `https://weather-and-climate.com/average-monthly-Rainfall-Temperature-Sunshine-in-Belgium`

[55] Vincenzo Liso, et al. (2018), *Modelling and Experimental Analysis of a Polymer Electrolyte Membrane Water Electrolysis Cell at Different Operating Temperatures*

6.1 Design A

6.1.1 Power per cell

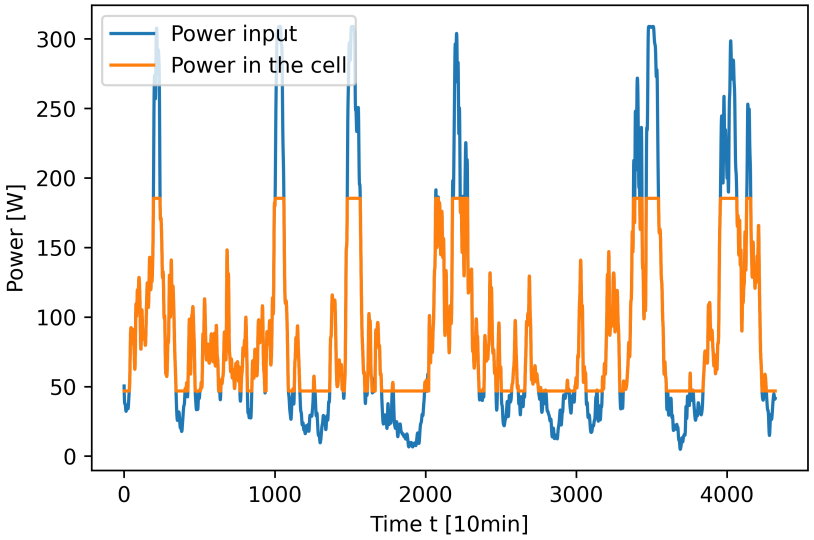

Figure 6.1: Power in the cell

6.1.2 Battery and grid activity

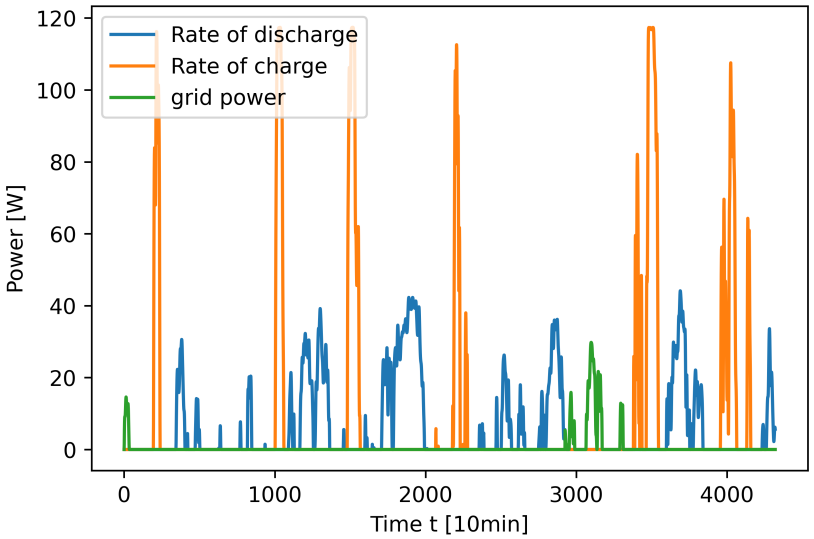

Figure 6.2: Charge and discharge rates of the battery and grid power

6.1.3 Energy stored in battery

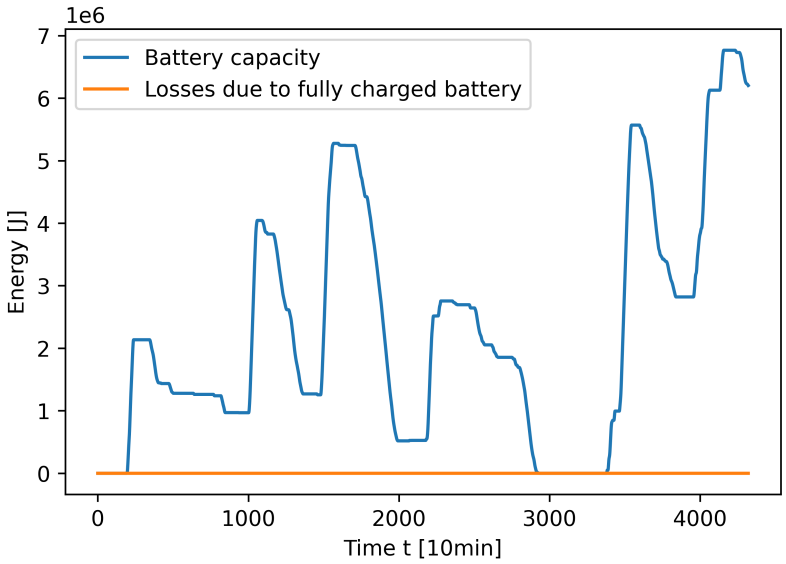

Figure 6.3: Energy stored in battery and losses due to fully charged battery

6.1.4 Current density in the cell

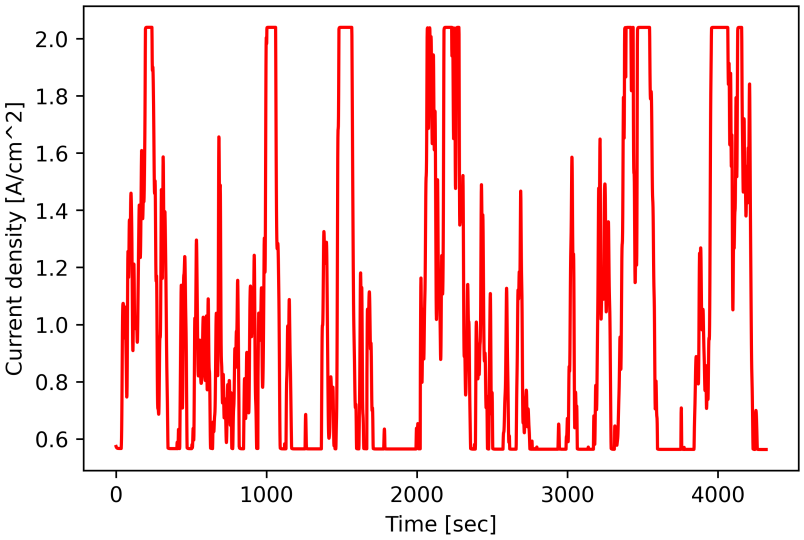

Figure 6.4: Current density in the cell

6.1.5 Dynamic regime detection variable

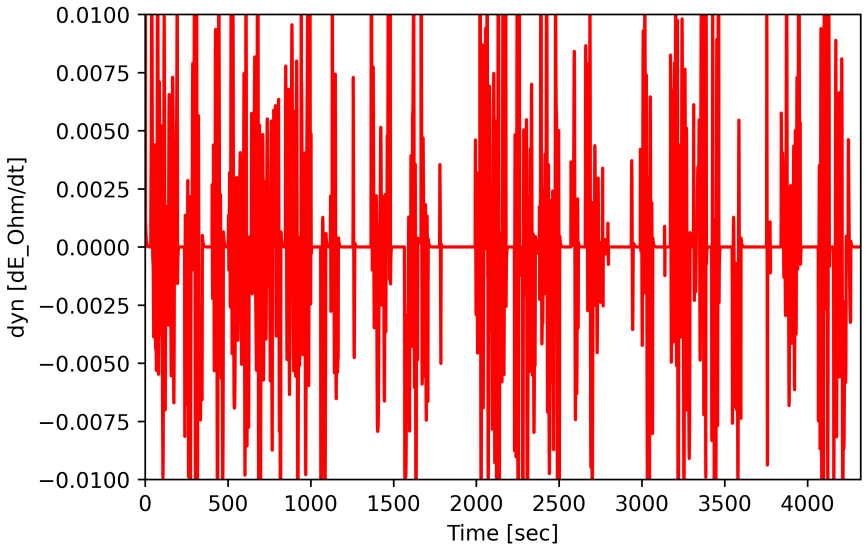

Figure 6.5: Evolution of the dynamic regime detection variable

6.1.6 Degradation of the cell

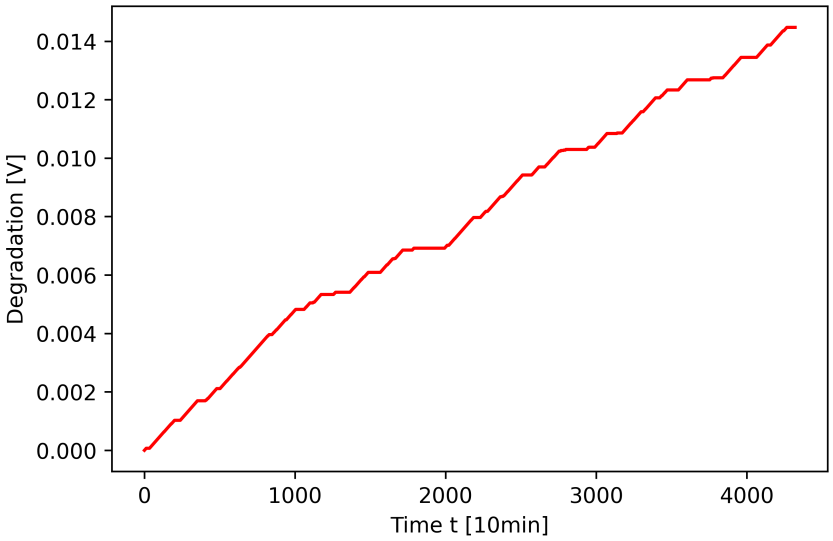

Figure 6.6: Degradation of the cell

6.1.7 Temperature in the cell

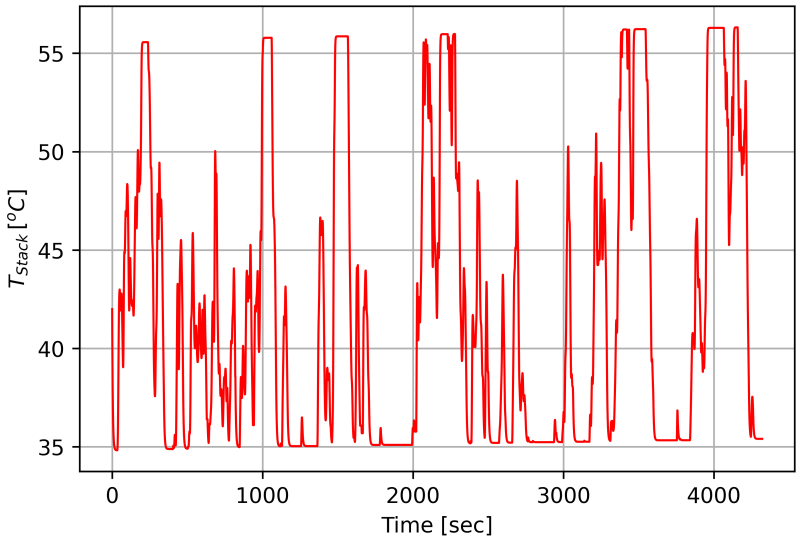

Figure 6.7: Temperature in the cell

6.1.8 Hydrogen production per cell

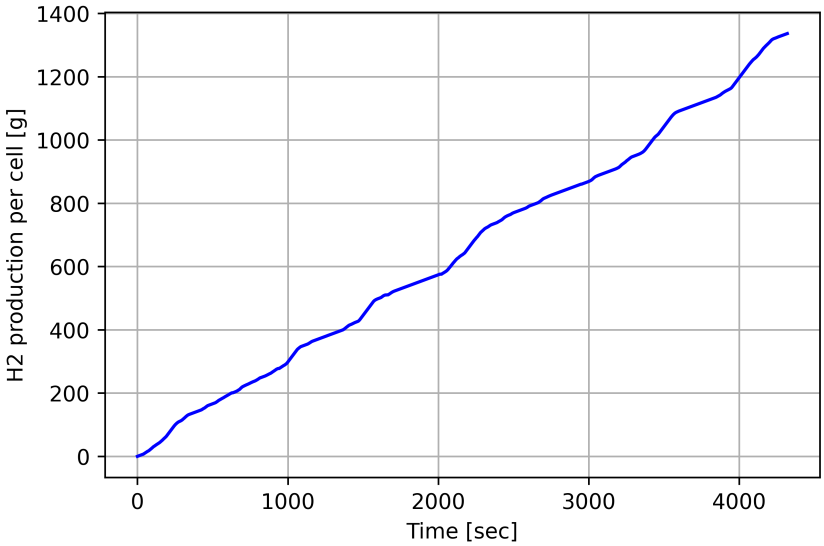

Figure 6.8: Hydrogen production per cell

6.2 Design B

6.2.1 Power per cell

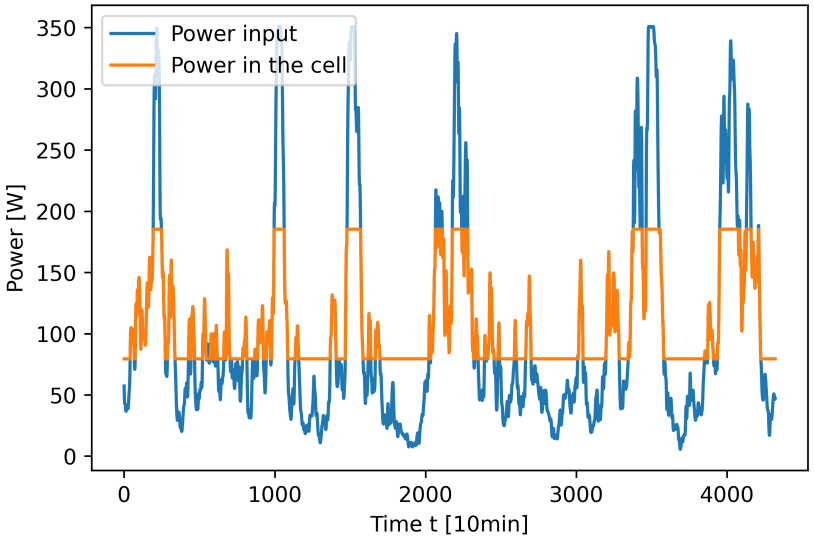

Figure 6.9: Power in the cell

6.2.2 Battery and grid activity

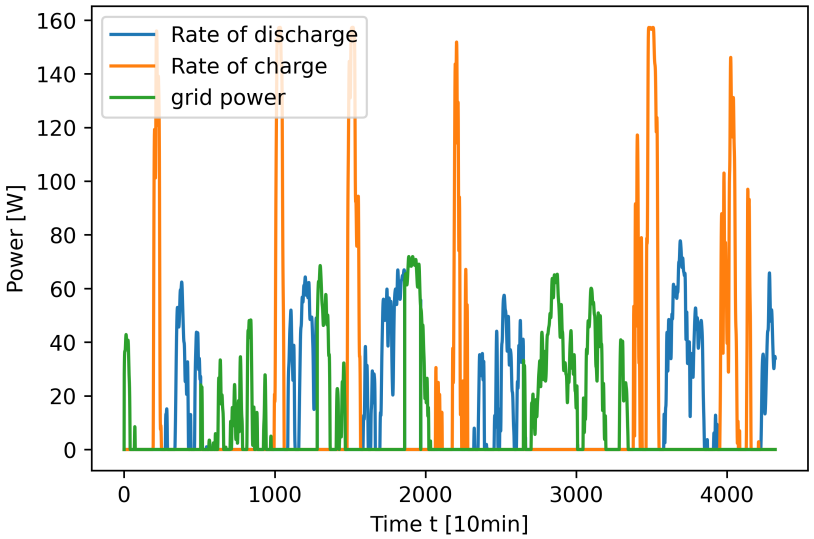

Figure 6.10: Charge and discharge rates of the battery and grid power

6.2.3 Energy stored in battery

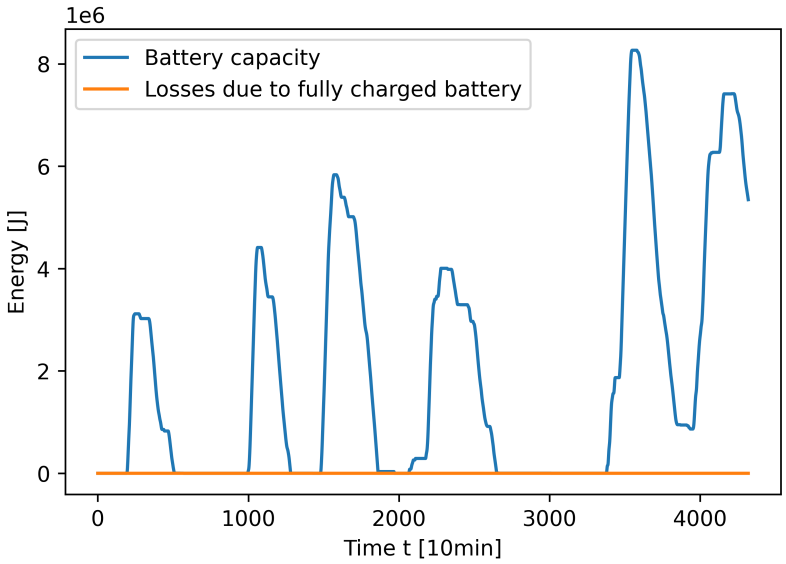

Figure 6.11: Energy stored in battery and losses due to fully charged battery

6.2.4 Current density in the cell

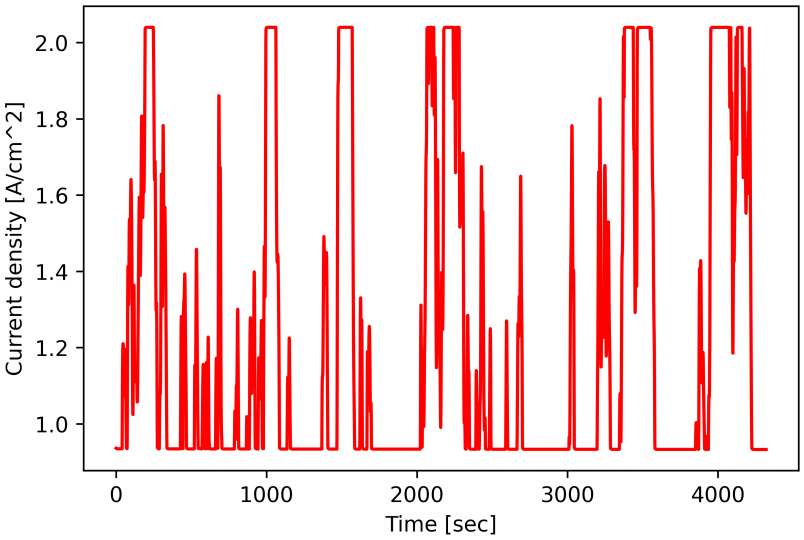

Figure 6.12: Current density in the cell

6.2.5 Dynamic regime detection variable

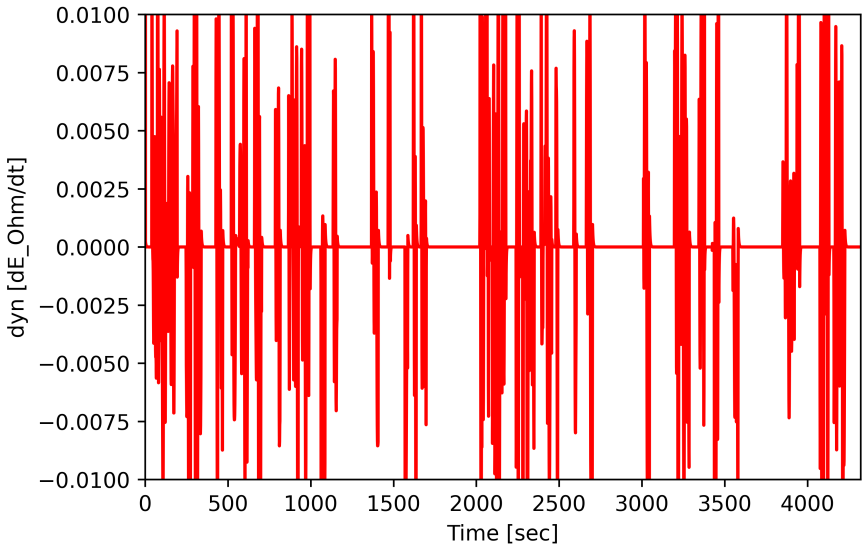

Figure 6.13: Evolution of the dynamic regime detection variable

6.2.6 Degradation of the cell

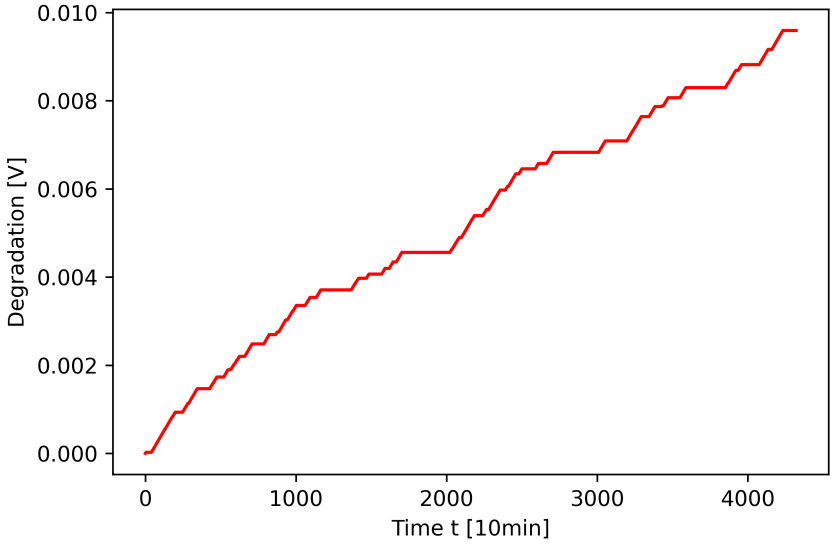

Figure 6.14: Degradation of the cell

6.2.7 Temperature in the cell

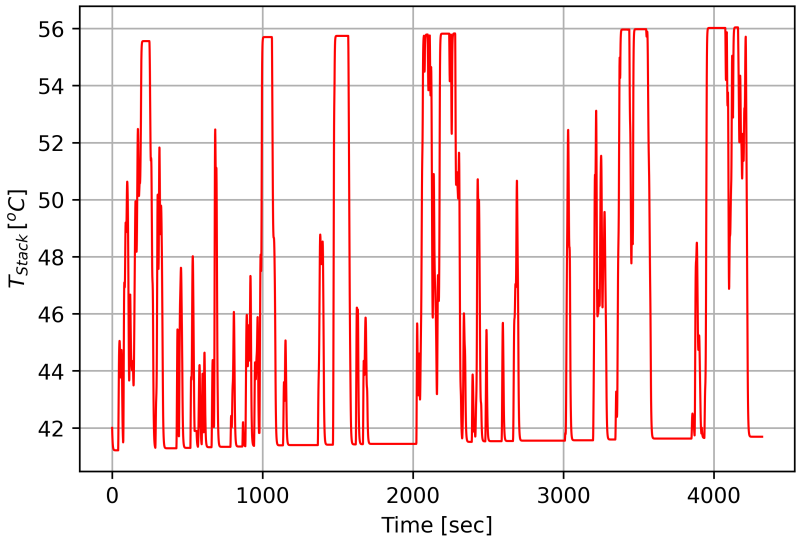

Figure 6.15: Temperature in the cell

6.2.8 Hydrogen production per cell

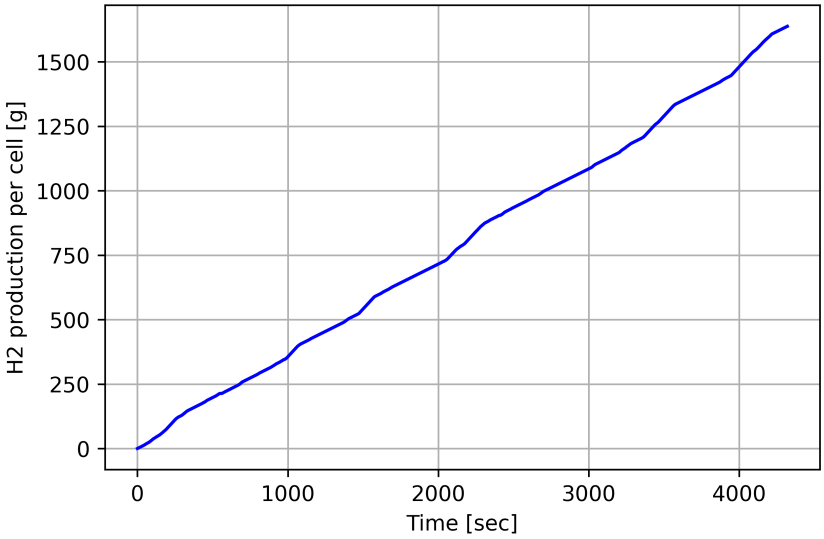

Figure 6.16: Hydrogen production per cell

6.3 System without batteries

6.3.1 Power per cell

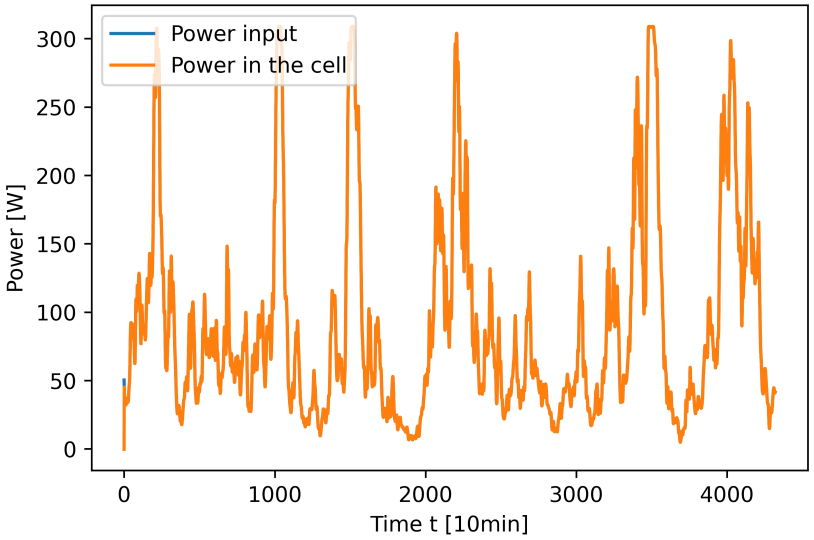

Figure 6.17: Power in the cell

6.3.2 Current density in the cell

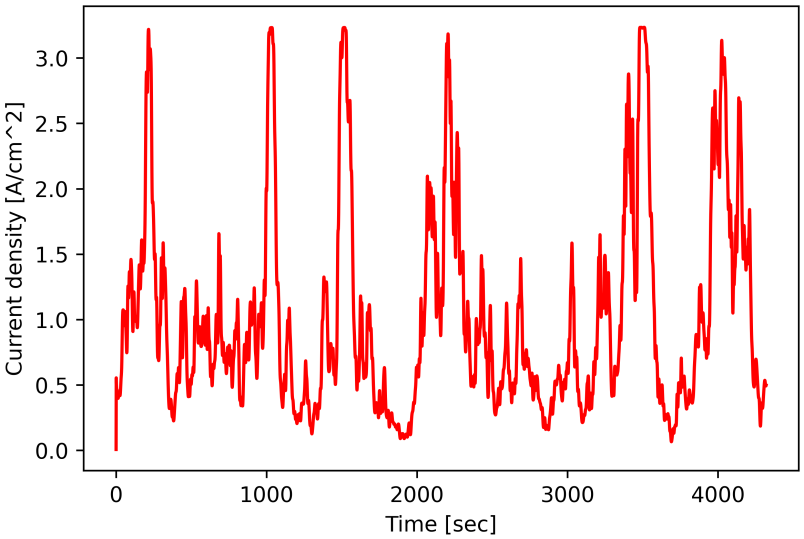

Figure 6.18: Current density in the cell

6.3.3 Dynamic regime detection variable

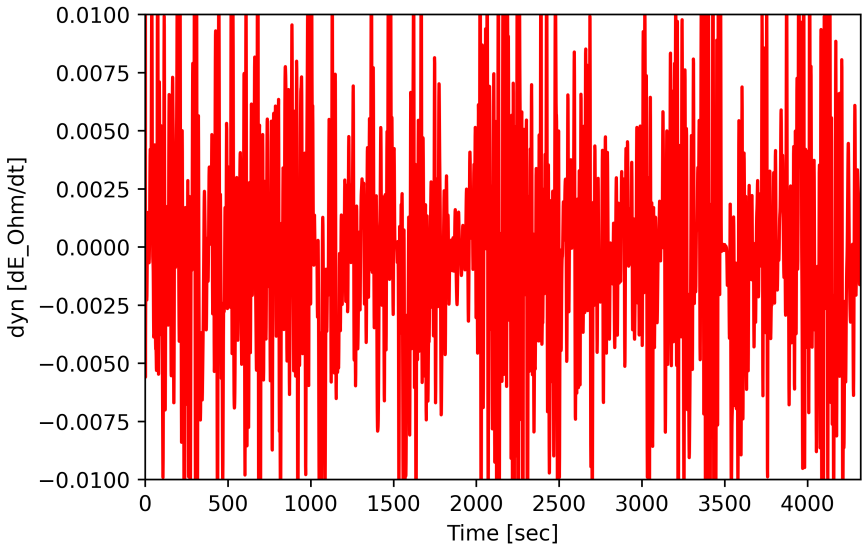

Figure 6.19: Evolution of the dynamic regime detection variable

6.3.4 Degradation of the cell

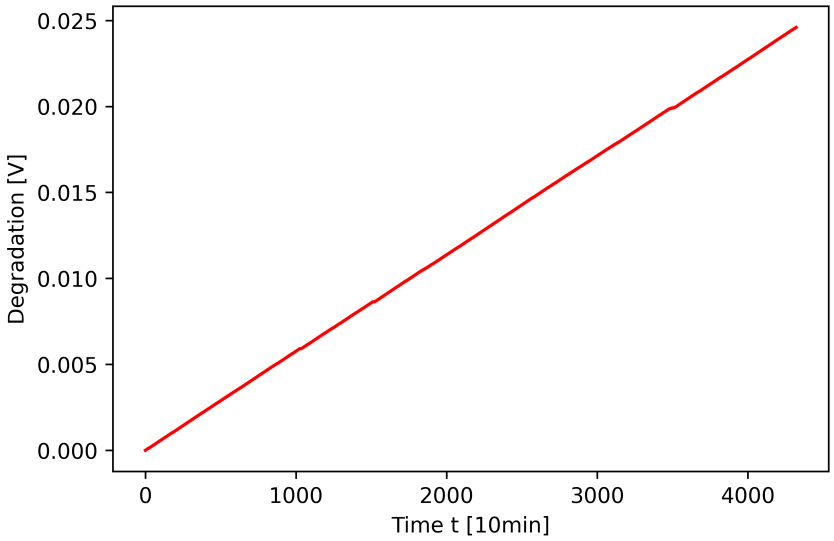

Figure 6.20: Degradation of the cell

6.3.5 Temperature in the cell

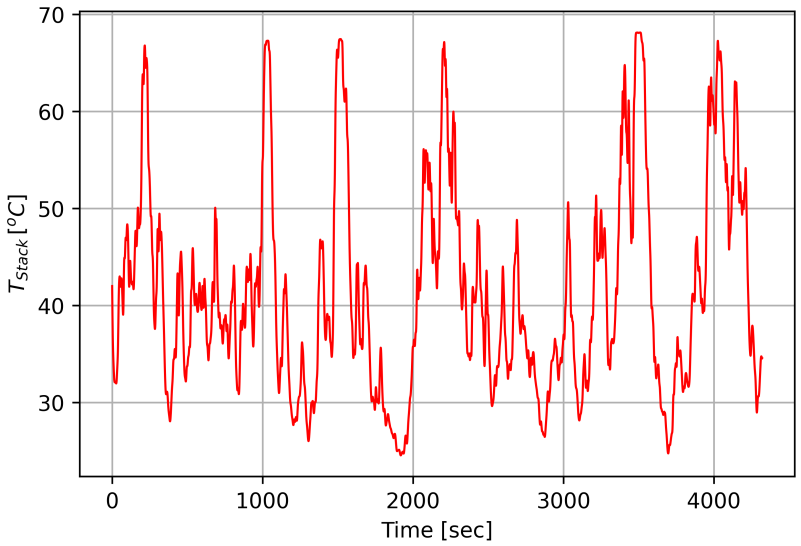

Figure 6.21: Temperature in the cell

6.3.6 Hydrogen production per cell

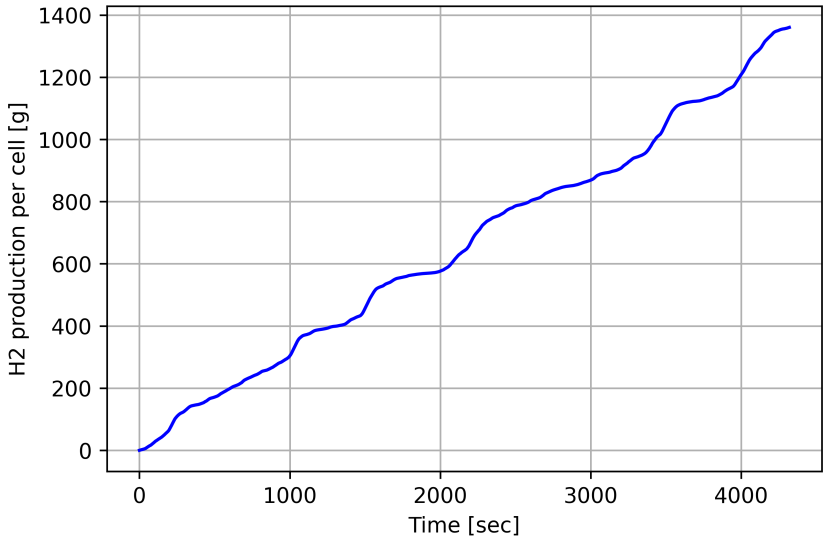

Figure 6.22: Hydrogen production per cell

UNIVERSITÉ CATHOLIQUE DE LOUVAIN
École polytechnique de Louvain
Rue Archimède, 1 bte L6.11.01, 1348 Louvain-la-Neuve, Belgique | **www.uclouvain.be/epl**